

Elastic wave propagation in anisotropic solids using energy-stable finite differences with weakly enforced boundary and interface conditions

Martin Almquist* Eric M. Dunham*,†

Abstract

Summation-by-parts (SBP) finite difference methods have several desirable properties for second-order wave equations. They combine the computational efficiency of narrow-stencil finite difference operators with provable stability on curvilinear multiblock grids. While several techniques for boundary and interface conditions exist, weak imposition via simultaneous approximation terms (SATs) is perhaps the most flexible one. Although SBP methods have been applied to elastic wave equations many times, an SBP-SAT method for general anisotropic elastic wave equations has not yet been presented in the literature. We fill this gap by deriving energy-stable self-adjoint SBP-SAT methods for general anisotropic materials on curvilinear multiblock grids. The methods are based on fully compatible SBP operators. We demonstrate the stability and accuracy properties of a particular set of fully compatible SBP-SAT schemes using the method of manufactured solutions. We also demonstrate the usefulness of the new method in elastodynamic cloaking and seismic imaging in mountainous regions.

1 Introduction

This paper considers numerical solution of elastic wave equations in complex geometries. We deal with the most general form of the anisotropic elastic wave equation (AEWE), which includes the isotropic elastic wave equation (IEWE) as a special case. Generally speaking, high-order finite difference methods are computationally efficient for wave-dominated equations with smooth solutions [22]. Finite difference (FD) operators with the summation-by-parts (SBP) property [24] lead to energy-stable discretizations on curvilinear multiblock grids when combined with suitable methods for imposing

*Department of Geophysics, Stanford University, Stanford, CA, USA

†Institute for Computational and Mathematical Engineering, Stanford University, Stanford, CA, USA

boundary and interface conditions. SBP FD methods may be used alone in moderately complex geometries, or as part of efficient hybrid solvers [25, 17] when unstructured meshing capabilities are required in parts of the domain. Recent applications of SBP methods to elastic wave equations include [40], which applied a second-order accurate scheme to tilted transversely isotropic media, and [48], which solved the first-order form of the IEWE. Another noteworthy contribution [13] introduced dual first-derivative SBP operators to solve the AEWE.

To minimize the number of unknowns, this paper discretizes the second-order form of the AEWE. For second order equations, narrow-stencil second-derivative SBP operators [29, 27] typically provide superior accuracy compared to applying a first-derivative operator twice. As a rule of thumb, the global convergence rate is one order higher [29] and the numerical dispersion relation mimics the exact dispersion relation better for marginally resolved modes [23]. Hence, we only consider narrow-stencil operators in this paper.

While SBP operators may be combined with various techniques for imposing boundary and interface conditions, weak enforcement via simultaneous approximation terms (SATs) [9] has proven competitive in a wide range of applications [11, 50]. The SBP-SAT combination is fully explicit and extends naturally to nonconforming grid blocks (see for example [28, 25, 3]) and nonlinear frictional interface conditions (see for example [20, 21]). We thus argue that there is value in furthering the SBP-SAT technique, even if alternative approaches exist. Previous works that used narrow-stencil SBP operators combined with other boundary treatments include [38, 15, 14]. In [38], Petersson and Sjögren presented a fourth order SBP scheme for the AEWE on curvilinear single-block grids. Boundary conditions were imposed with a ghost-point technique. In [15], Duru and Virta presented an SBP-SAT scheme for the IEWE on curvilinear multiblock grids. Traction boundary conditions were imposed using SATs and displacement boundary conditions were strongly enforced, using the injection method [14]. Herein, we construct an SBP-SAT method for the AEWE on curvilinear multiblock grids. Robin boundary conditions (which include traction conditions), displacement boundary conditions, and interface conditions, are all imposed using SATs. We prove that the spatial discretization is energy stable and self-adjoint.

The methods derived in this paper are based on *fully compatible* diagonal-norm second-derivative SBP operators [30] (see Section 4 for the definition). The assumption of full compatibility greatly simplifies the stability analysis when using SATs to impose displacement boundary conditions and inter-block couplings. The significant simplifications facilitated by the fully compatible operators were noted in [15] for the IEWE, and later in [2] for the acoustic wave equation. The fully compatible operators are to be contrasted with *compatible* operators, which are more commonly used. The compatible operators constructed by Mattsson in [27] with interior order $2q$ have bound-

ary closures of order q and boundary derivative operators of order $q+1$, yielding $(q+2)$ th order global accuracy in most numerical experiments. Fisher and Carpenter [16] constructed a fully compatible $2q = 4$ operator with q th order closures and boundary derivatives of order q . The reduction of the boundary derivative order (compared to Mattsson's compatible operators) increases the local truncation error by one order for Neumann-type boundary conditions and inter-block couplings. To the best of our knowledge, fully compatible operators for variable coefficients with q th order boundary closures and $(q+1)$ th order boundary derivative operators are not yet available in the literature. We strongly encourage efforts to construct such operators. Until they become available, we resort to so-called *adapted* fully compatible operators, which can be constructed from any set of compatible operators [14] (see Section 4). The adapted operators are identical to the original operators except at the first and last grid points, where the accuracy is reduced to $(q-1)$ th order. By the general result in [49], we expect the ℓ^2 error of pointwise stable schemes to be of order $\min(q_b + 2, 2q)$, where q_b denotes the boundary accuracy. This implies that the adapted operators might yield up to one order lower convergence rates than the corresponding compatible operators. Remarkably, however, experiments with the IEWE in [15] showed no loss in convergence rates. The adapted $2q = 6$ operator even yielded smaller errors than the original operator. Although a theoretical explanation of this super convergence is currently lacking, the adapted operators seem attractive from a practical point of view. In this paper, we investigate how the adapted operators fare when applied to the AEWE.

The rest of this paper is organized as follows. We introduce notational conventions in Section 2. In Section 3, we review the equations of linear anisotropic elasticity and discuss how they change under coordinate transformations. We introduce compatible and adapted fully compatible SBP operators in Section 4, and combine them with proper SATs to construct energy-stable self-adjoint schemes for Robin and displacement boundary conditions in Section 5. In Section 6, we derive SATs for grid-block couplings. Numerical experiments are presented in Section 7. We evaluate the convergence rates of the new multi-block SBP-SAT scheme against a manufactured solution and show the applicability of the scheme in elastodynamic cloaking and seismic imaging of the Earth. Conclusions follow in Section 8.

2 Notation conventions

Let $\Omega \subset \mathbb{R}^d$ denote a bounded domain in d dimensions and let $u, v \in L^2(\Omega)$. We use the L^2 inner product:

$$(u, v)_\Omega = \int_\Omega uv \, d\Omega. \quad (1)$$

Similarly, we use the notation

$$(u, v)_{\partial\Omega} = \int_{\partial\Omega} uv \, dS \quad (2)$$

for surface integrals. Note, however, that $(\cdot, \cdot)_{\partial\Omega}$ is not an inner product but a bilinear form. We use the summation convention for repeated subscript indices so that

$$u_i v_i = \sum_{i=1}^d u_i v_i. \quad (3)$$

The summation convention applies to inner products too, i.e.,

$$(u_i, v_i) = \sum_{i=1}^d (u_i, v_i). \quad (4)$$

The summation convention only applies to indices $i, j, k, \ell, m, I, J, K$, and L . In particular, it does not apply to x, γ , or N .

Boldface font is reserved for vectors \mathbf{u} whose elements approximate some scalar field u evaluated on the grid. We will later define discrete inner products and use the summation convention in the discrete setting too, so that

$$(\mathbf{u}_i, \mathbf{v}_i) = \sum_{i=1}^d (\mathbf{u}_i, \mathbf{v}_i). \quad (5)$$

For all spatially variable coefficients, we use the same symbol also in the discrete case, which then is understood to denote a diagonal matrix with the values of that coefficient on the diagonal. The outward unit normals \hat{n} and $\hat{\nu}$ (see Figure 1) are regarded as variable coefficients that take non-zero values only at boundary points. In the discrete setting, the values of \hat{n} and $\hat{\nu}$ at edge and corner points change with context. When integrating over a face, \hat{n} (or $\hat{\nu}$) is understood to denote the unit normal to that face even at edge and corner points. The same convention applies to the surface area scale factor \hat{J} .

3 Equations of linear elasticity

Let $\{\vec{E}_I\}$ denote an orthonormal basis in \mathbb{R}^d , let $\vec{X} = X_I \vec{E}_I$, and let $\partial_I = \partial/\partial X_I$. The generalized Hooke's law for an elastic medium relates stress to strain and reads

$$\sigma_{IJ} = C_{IJKL} \partial_K u_L, \quad (6)$$

where u_L is the displacement vector, σ_{IJ} is the stress tensor, and C_{IJKL} is the elastic stiffness tensor. The stiffness tensor has the major symmetry

$$C_{IJKL} = C_{KLIJ}. \quad (7)$$

Normal elastic materials also have the minor symmetry

$$C_{ijkl} = C_{jikl}, \quad (8)$$

which implies that the stress tensor is symmetric, i.e., $\sigma_{ij} = \sigma_{ji}$. In this paper, we consider the more general theory of Cosserat elasticity [10], in which stress is not necessarily symmetric. That is, we do not assume that the stiffness tensor has the minor symmetry (8). Requiring a non-negative elastic strain energy density results in the condition

$$S_{ij} C_{ijkl} S_{kl} \geq 0 \quad \forall S_{ij}, \quad (9)$$

which we assume that C_{ijkl} satisfies. The momentum balance reads

$$\rho \ddot{u}_j = \partial_i \sigma_{ij} + f_j, \quad (10)$$

where ρ is density and f_j denotes external body forces. Substituting Hooke's law (6) in (10) yields the elastic wave equation for displacements,

$$\begin{aligned} \rho \ddot{u}_j &= \partial_i C_{ijkl} \partial_k u_l + f_j, & \vec{X} \in \Omega, \\ L_{ij} u_j &= 0, & \vec{X} \in \partial\Omega, \end{aligned} \quad (11)$$

where $\Omega \subset \mathbb{R}^d$ is a bounded domain with outward unit normal $\hat{n} = n_i \vec{E}_i$ and the linear operator L_{ij} represents well-posed boundary conditions. The traction vector $\vec{\tau} = \tau_j \vec{E}_j$ acting on $\partial\Omega$ is

$$\tau_j = n_i \sigma_{ij} = n_i C_{ijkl} \partial_k u_l. \quad (12)$$

For future use we define the traction operator

$$T_{jl} = n_i C_{ijkl} \partial_k \quad (13)$$

such that $\tau_j = T_{jl} u_l$.

In the absence of external body forces, the energy method, which amounts to multiplying the first equation in (11) by \dot{u}_j and integrating over Ω , leads to

$$\begin{aligned} (\dot{u}_j, \rho \ddot{u}_j)_\Omega &= (\dot{u}_j, \partial_i C_{ijkl} \partial_k u_l)_\Omega \\ &= (\dot{u}_j, n_i C_{ijkl} \partial_k u_l)_{\partial\Omega} - (\partial_i \dot{u}_j, C_{ijkl} \partial_k u_l)_\Omega \\ &= (\dot{u}_j, \tau_j)_{\partial\Omega} - (\partial_i \dot{u}_j, C_{ijkl} \partial_k u_l)_\Omega, \end{aligned} \quad (14)$$

where we used integration by parts and the definition of τ_j . We have

$$(\dot{u}_j, \rho \ddot{u}_j)_\Omega = \frac{1}{2} \frac{d}{dt} (\dot{u}_j, \rho \dot{u}_j)_\Omega. \quad (15)$$

The major symmetry of the stiffness tensor (7) yields

$$(\partial_i \dot{u}_j, C_{ijkl} \partial_k u_l)_\Omega = (\partial_k \dot{u}_l, C_{ijkl} \partial_i u_j)_\Omega = \frac{1}{2} \frac{d}{dt} (\partial_i u_j, C_{ijkl} \partial_k u_l)_\Omega. \quad (16)$$

The total energy \mathcal{E} is the sum of kinetic and strain energy,

$$\mathcal{E} = \frac{1}{2} (\dot{u}_J, \rho \dot{u}_J)_\Omega + \frac{1}{2} (\partial_I u_J, C_{IJKL} \partial_K u_L)_\Omega. \quad (17)$$

The positive semidefiniteness of the stiffness tensor (9) ensures that the strain energy is non-negative. Rearranging terms in (14) leads to the energy rate

$$\frac{d\mathcal{E}}{dt} = (\dot{u}_J, \tau_J)_{\partial\Omega}. \quad (18)$$

We note that homogeneous displacement boundary conditions ($u_J = 0$) and homogeneous traction boundary conditions ($\tau_J = 0$) both yield energy conservation.

3.1 Coordinate transformation

Let $\{\vec{e}_i\}$ denote an orthonormal basis in \mathbb{R}^d and let $\vec{x} = x_i \vec{e}_i$. Introduce a smooth one-to-one mapping $X_I = X_I(x_1, \dots, x_d)$ from the reference domain $\omega = [0, 1]^d$ to the physical domain Ω , as illustrated in Figure 1. We will use

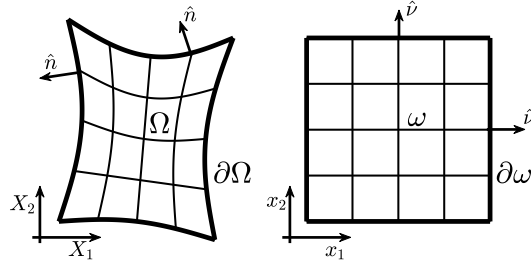


Figure 1: Schematic of the physical domain Ω and the reference domain ω

uppercase letters for quantities related to the physical domain and lowercase letters for similar quantities in the reference domain. We define $\partial_i = \partial/\partial x_i$. Let

$$F_{Ii} = \partial x_i / \partial X_I \quad (19)$$

denote the transformation gradient and let

$$J = \det[F_{Ii}] \quad (20)$$

denote the Jacobian of the transformation. We assume $J > 0$. Note that the object F_{Ii} is not a second order tensor because it maps from one domain to the other [33]. By the chain rule,

$$\partial_I = F_{Ii} \partial_i. \quad (21)$$

The following metric identities are well known (see [52]):

$$J F_{Ii} \partial_i = \partial_i J F_{Ii}. \quad (22)$$

Let \vec{a}_i denote the covariant basis vectors:

$$\vec{a}_i = \partial_i \vec{X} = \partial_i X_I \vec{E}_I = (F^{-1})_{iI} \vec{E}_I. \quad (23)$$

3.1.1 Transforming the PDE

Using first (21) and then (22), we have

$$\partial_I C_{IJKL} \partial_K = F_{Ii} \partial_i C_{IJKL} F_{Kk} \partial_k = J^{-1} \partial_i F_{Ii} J C_{IJKL} F_{Kk} \partial_k. \quad (24)$$

Introduce a change of variables

$$u_I = A_{Ii} u_i, \quad \tau_I = A_{Ii} \tau_i, \quad (25)$$

for some A_{Ii} to be discussed later. We can now write the equations of motion in (11) as

$$J \rho \ddot{u}_j = (A^{-1})_{jJ} \partial_i F_{Ii} J C_{IJKL} F_{Kk} \partial_k A_{L\ell} u_\ell + J (A^{-1})_{jJ} f_j. \quad (26)$$

In this paper we will use the trivial change of variables

$$A_{Ii} = \delta_{Ii}, \quad (27)$$

which yields the equations of motion

$$J \rho \ddot{u}_j = \partial_i F_{Ii} J C_{IJKL} F_{Kk} \partial_k u_\ell + J f_j. \quad (28)$$

Define the transformed density and stiffness tensor

$$\varrho = J \rho, \quad c_{ijk\ell} = F_{Ii} J C_{IJKL} F_{Kk}. \quad (29)$$

The transformed equation, posed on the unit cube ω , reads

$$\begin{aligned} \varrho \ddot{u}_j &= \partial_i c_{ijk\ell} \partial_k u_\ell + J f_j, & \vec{x} \in \omega, \\ \Lambda_{ij} u_j &= 0, & \vec{x} \in \partial\omega, \end{aligned} \quad (30)$$

where Λ_{ij} denotes the transformation of L_{IJ} . Using the definition of $c_{ijk\ell}$ in (24) shows that

$$\partial_I C_{IJKL} \partial_K = J^{-1} \partial_i c_{ijk\ell} \partial_k. \quad (31)$$

In Section 4 we use formula (31) to construct an SBP operator that approximates $\partial_I C_{IJKL} \partial_K$.

The transformed stiffness tensor retains the major symmetry,

$$c_{k\ell ij} = F_{Ik} J C_{i\ell Kj} F_{Ki} = F_{Ik} J C_{Kj\ell K} F_{Ki} = F_{Kk} J C_{1j\ell K} F_{Ki} = c_{ijk\ell}, \quad (32)$$

and the semidefiniteness

$$s_{ij} c_{ijk\ell} s_{k\ell} = \underbrace{s_{ij} F_{Ii}}_{=: S_{Ij}} J C_{IJKL} \underbrace{F_{Kk} s_{k\ell}}_{=: S_{K\ell}} \geq 0 \quad \forall s_{ij}, \quad (33)$$

where we used the semidefiniteness of C_{IJKL} (9) and the positivity of J . We conclude that the transformed PDE is of the same form as the original PDE

in (11). However, even if C_{ijkl} has the minor symmetry (8), the transformed stiffness tensor generally does not, because

$$\begin{aligned} c_{ijkl} - c_{jikl} &= F_{ii}JC_{ijkl}F_{kk} - F_{ij}JC_{iikl}F_{kk} \\ &= (F_{ii}C_{ijkl} - F_{ij}C_{iikl}) JF_{kk} \\ &= (F_{ii}C_{ijkl} - F_{ij}C_{iikl}) JF_{kk}, \end{aligned} \quad (34)$$

which is nonzero, in general. Hence, the equations of Cosserat materials are invariant under coordinate transformations, but the equations of normal materials are not. It is, however, possible to symmetrize the effective transformed stress tensor by setting (see [33] for a thorough discussion of coordinate transformations in elastic wave equations)

$$A_{ii} = F_{ii}. \quad (35)$$

This approach introduces additional terms in the transformed equations of motion, similar to those required for Willis materials [31, 32], and will not be pursued in the present study.

In the semidiscrete stability proof we will make use of the property

$$u_j c_{mjml} u_\ell \geq 0 \quad \forall u_j, \quad (36)$$

which follows from (33), because

$$u_j c_{mjml} u_\ell = \underbrace{u_j \delta_{im}}_{=:U_{ijm}} \underbrace{c_{ijkl}}_{=:U_{k\ell m}} \underbrace{u_\ell \delta_{km}}_{\geq 0 \forall m} = \sum_m \underbrace{U_{ijm} c_{ijkl} U_{k\ell m}}_{\geq 0} \geq 0. \quad (37)$$

3.1.2 Integrals and normals

Since $Jd\omega$ is the volume element, we have $d\Omega = Jd\omega$, and hence

$$(u, v)_\Omega = (u, Jv)_\omega. \quad (38)$$

Similarly, we let \hat{J} denote the surface area scale factor such that

$$(u, v)_{\partial\Omega} = (u, \hat{J}v)_{\partial\omega}. \quad (39)$$

The surface area scale factor \hat{J} is related to the covariant basis vectors \vec{a}_i defined in (23) as follows. In two space dimensions

$$\hat{J} = |\vec{a}_i|, \quad x_j \in \{0, 1\}, \quad i, j \text{ cyclic}, \quad (40)$$

and in three space dimensions

$$\hat{J} = |\vec{a}_i \times \vec{a}_j|, \quad x_k \in \{0, 1\}, \quad i, j, k \text{ cyclic}. \quad (41)$$

Let $\hat{\nu} = \nu_i \vec{e}_i$ denote the unit normal to ω . The normals \hat{n} and $\hat{\nu}$ are related by Nanson's formula [26],

$$\hat{J} n_i = J F_{ii} \nu_i. \quad (42)$$

3.2 Numerical approximation of the transformation gradient

In this subsection we comment briefly on how numerical approximations of properties of the coordinate transformation may be computed. We compute an approximation $\underline{F}_{ii} \approx \underline{F}_{ii}$ of the transformation gradient by applying derivative approximations to a given grid. To retain the order of accuracy, \underline{F}_{ii} needs to be at least as accurate as the finite difference operators used to discretize the PDE. Higher-order approximations, or even the exact \underline{F}_{ii} , if available, could also be used. For all numerical experiments in this paper, we compute \underline{F}_{ii} using first-derivate SBP operators of the same order as we use to solve the PDE. That is, \underline{F}_{ii} is computed to order q near boundaries and order $2q$ in the interior.

Once \underline{F}_{ii} is computed, we use relations between the corresponding continuous quantities to define all other approximations. We set

$$\underline{J} = \det[\underline{F}_{ii}], \quad (43)$$

$$\underline{c}_{ijkl} = \underline{F}_{ii} \underline{J} \underline{C}_{ijkl} \underline{F}_{kk}, \quad (44)$$

$$\vec{a}_i = (\underline{F}^{-1})_{ii} \vec{E}_i, \quad (45)$$

$$\hat{J} = |\vec{a}_i|, \quad x_j \in \{0, 1\}, \quad i, j \text{ cyclic, (in 2D)}, \quad (46)$$

or

$$\hat{J} = |\vec{a}_i \times \vec{a}_j|, \quad x_k \in \{0, 1\}, \quad i, j, k \text{ cyclic, (in 3D)}, \quad (47)$$

and

$$n_i = \hat{J}^{-1} \underline{J} \underline{F}_{ii} \nu_i. \quad (48)$$

The only requirements for stability of the semidiscrete scheme (to be introduced later) are $\underline{J} > 0$, $\underline{c}_{ijkl} = \underline{c}_{klij}$, $s_{ij} \underline{c}_{ijkl} s_{kl} \geq 0 \ \forall s_{ij}$, and $\hat{J} > 0$. We suggest checking the condition $\underline{J} > 0$, which could be violated due to truncation errors. Assuming $\underline{J} > 0$, the remaining three conditions are guaranteed to be satisfied, regardless of how \underline{F}_{ii} was computed, because

$$\underline{c}_{klij} = \underline{F}_{ik} \underline{J} \underline{C}_{lKj} \underline{F}_{Ki} = \underline{F}_{ik} \underline{J} \underline{C}_{Kjl} \underline{F}_{Ki} = \underline{F}_{kk} \underline{J} \underline{C}_{ijkl} \underline{F}_{ii} = \underline{c}_{ijkl}, \quad (49)$$

$$s_{ij} \underline{c}_{ijkl} s_{kl} = \underbrace{s_{ij} \underline{F}_{ii}}_{=: S_{ij}} \underline{J} \underline{C}_{ijkl} \underbrace{\underline{F}_{kk} s_{kl}}_{=: S_{Kl}} \geq 0 \quad \forall s_{ij}, \quad (50)$$

and $\hat{J} > 0$ follows from formulas (46) and (47), combined with the assumption $\underline{J} > 0$, which implies that \underline{F}_{ii} is nonsingular and thus guarantees $\vec{a}_i \neq \vec{0}$.

Note that since we used Nanson's formula (42) to define \hat{n} , Nanson's formula holds identically for the approximated quantities. We conclude that \underline{F}_{ii} may be computed with any sufficiently accurate method, as long as the resulting Jacobian is positive. With a slight abuse of notation, we henceforth drop the underline notation and let it be implied that we may be dealing with approximations in the discrete setting.

3.2.1 The transformed stiffness tensor of isotropic materials

Isotropic materials are characterized by the two Lamé parameters λ and μ and have the stiffness tensor

$$C_{ijkl} = \lambda \delta_{ij} \delta_{kl} + \mu (\delta_{ik} \delta_{jl} + \delta_{il} \delta_{jk}). \quad (51)$$

The isotropic stiffness tensor transforms into

$$\begin{aligned} c_{ijkl} &= F_{ii} J C_{ijkl} F_{kk} = F_{ii} J [\lambda \delta_{ij} \delta_{kl} + \mu (\delta_{ik} \delta_{jl} + \delta_{il} \delta_{jk})] F_{kk} \\ &= J [\lambda F_{ji} F_{\ell k} + \mu (F_{ki} \delta_{jl} F_{kk} + F_{\ell i} F_{jk})]. \end{aligned} \quad (52)$$

In 3D, there are 9 independent parameters in F_{ii} , which leads to a total of 11 independent parameters in c_{ijkl} . In general, the transformed stiffness tensor does not have the minor symmetry even in the isotropic case, because

$$\begin{aligned} c_{ijkl} - c_{jikl} &= J \lambda (F_{ji} - F_{ij}) J F_{\ell k} \\ &\quad + J \mu [(F_{ki} \delta_{jl} - F_{kj} \delta_{il}) F_{kk} + F_{\ell i} F_{jk} - F_{\ell j} F_{ik}], \end{aligned} \quad (53)$$

which is nonzero in general.

4 Summation-by-parts operators

Most of the definitions in this section are not new but are restated here for completeness. The notation follows [2] closely. We consider only diagonal-norm SBP operators. That is, the so-called norm matrix H_x has the structure

$$H_x = \text{diag}(h_1, h_2, \dots, h_2, h_1), \quad (54)$$

where all h_i are proportional to the grid spacing h . The first-derivative SBP operators $D_x \approx \partial_x$ have the integration-by-parts-mimicking property

$$H_x D_x = -D_x^T H_x - e_0 e_0^T + e_N e_N^T, \quad (55)$$

where the vectors e_0 and e_N interpolate or extrapolate to the left and right boundaries, respectively. We herein restrict our attention to grids that include the boundary points of the interval $[x_L, x_R]$, in which case one may set

$$e_0 = [1, 0, \dots, 0]^T, \quad e_N = [0, \dots, 0, 1]^T. \quad (56)$$

We will use the first-derivative operators presented in [29], which (for orders $2q \geq 6$) correspond to a particular choice of the free parameters in the operators developed in [24, 44, 34, 47]. The *compatible* narrow-stencil second-derivative operators $D_{xx}(b) \approx \partial_x b \partial_x$ derived in [27] are based on the same norm matrix H_x and have the property

$$H_x D_{xx}(b) = -D_x^T H_x b D_x - R_{xx}(b) - e_0 e_0^T b \hat{D}_x + e_N e_N^T b \hat{D}_x, \quad (57)$$

where the first and last rows of \hat{D}_x approximate the first derivative and the interior of \hat{D}_x is zero (\hat{D}_x was denoted S in [27]). Note that for the SBP operators derived in [27], $e_{0,N}^T D_x \neq e_{0,N}^T \hat{D}_x$. If $e_{0,N}^T D_x = e_{0,N}^T \hat{D}_x$, then the SBP operators D_x and D_{xx} are said to be *fully compatible* [30]. The SBP operators derived in [27] have \hat{D}_x that are accurate of order $q + 1$, i.e., one order higher than the boundary closure of D_x .

The matrix $R_{xx}(b)$ is symmetric positive semidefinite and consists of undivided difference approximations in such a way that $\mathbf{u}^T R_{xx}(b) \mathbf{v}$ is zero to order $2q$ [27]. Its structure is

$$R_{xx}(b) = \sum_{\alpha} h^{2\alpha-2} D_{x^\alpha}^T E_{\alpha}^T H_x B_{\alpha}(b) E_{\alpha} D_{x^\alpha}, \quad (58)$$

where $\alpha \geq q + 1$; $D_{x^\alpha} \approx \partial^\alpha / \partial x^\alpha$; the E_α are of order 1; and the B_α are diagonal matrices whose entries are convex combinations of $b(x)$ evaluated on the grid. Let b_s denote b evaluated at the s th grid point, and let $(B_\alpha)_s$ denote the entry in B_α associated with the s th grid point. The structure of $B_\alpha(b)$ is

$$(B_\alpha(b))_r = \sum_s \beta_{\alpha,r,s} b_s, \quad \beta_{\alpha,r,s} \geq 0 \quad \forall \alpha, r, s. \quad (59)$$

To simplify the notation we define

$$\mathcal{D}_{x^\alpha} = h^{\alpha-1} H_x^{1/2} E_\alpha D_{x^\alpha} \quad (60)$$

such that

$$R_{xx}(b) = \sum_{\alpha} \mathcal{D}_{x^\alpha}^T B_\alpha(b) \mathcal{D}_{x^\alpha}. \quad (61)$$

For future use we prove the following lemma, which states that R_{xx} preserves semidefiniteness of two-tensors.

Lemma 1. *If $u_i S_{ij} u_j \geq 0 \forall u_i$, then*

$$\mathbf{u}_i R_{xx}(S_{ij}) \mathbf{u}_j \geq 0 \quad \forall \mathbf{u}_i. \quad (62)$$

Proof.

$$\begin{aligned} \mathbf{u}_i R_{xx}(S_{ij}) \mathbf{u}_j &= \sum_{\alpha} (\mathcal{D}_{x^\alpha} \mathbf{u}_i)^T B_\alpha(S_{ij}) \mathcal{D}_{x^\alpha} \mathbf{u}_j \\ &= \sum_{\alpha,r} (\mathcal{D}_{x^\alpha} \mathbf{u}_i)_r (B_\alpha(S_{ij}))_r (\mathcal{D}_{x^\alpha} \mathbf{u}_j)_r \quad [\text{Use (59)}] \\ &= \sum_{\alpha,r,s} (\mathcal{D}_{x^\alpha} \mathbf{u}_i)_r \beta_{\alpha,r,s} (S_{ij})_s (\mathcal{D}_{x^\alpha} \mathbf{u}_j)_r \quad [\text{Use } u_i S_{ij} u_j \geq 0] \\ &\geq 0. \end{aligned} \quad (63)$$

□

In particular, Lemma 1 shows that R_{xx} preserves the semidefiniteness of the two-tensor $c_{mjm\ell}$ (cf. (36)):

$$\mathbf{u}_j R_{xx}(c_{mjm\ell}) \mathbf{u}_\ell \geq 0 \quad \forall \mathbf{u}_j. \quad (64)$$

4.1 Adapted fully compatible SBP operators

Any compatible second-derivative operator can be turned into a fully compatible operator, here denoted D_{xx}^{FC} , by simply replacing the boundary derivatives \hat{D}_x by D_x [15]. We refer to such operators as *adapted* fully compatible operators. For the operators derived in [27], swapping boundary derivatives amounts to adding terms of order $q - 1$ at the grid end points,

$$D_{xx}^{\text{FC}} = D_{xx} + \underbrace{H_x^{-1} \left(e_0 e_0^T b(\hat{D}_x - D_x) \right)}_{\mathcal{O}(h^{q-1})} - \underbrace{H_x^{-1} \left(e_N e_N^T b(\hat{D}_x - D_x) \right)}_{\mathcal{O}(h^{q-1})}. \quad (65)$$

Hence, the adapted fully compatible operators are one order less accurate than the original operators at precisely one grid point at each boundary. It is not obvious how the local reduction in accuracy affects the global convergence rate. A pessimist would expect reduction by a full order, but [15] did not observe any reduction for isotropic elasticity. Our numerical experiments in Section 7 indicate a reduction by half an order for orders $2q = 4$ and $2q = 6$, and no reduction for $2q = 2$, for anisotropic materials.

In the following derivations we shall assume fully compatible operators. This assumption greatly simplifies the stability proofs (for a discussion on how non-fully compatible operators complicate the stability proofs for the acoustic wave equation, see [2]). In all numerical experiments we will use the adapted fully compatible operators.

4.2 Positivity properties

It follows immediately from (54) and (56) that we have

$$H_x = \text{diag}(0, h_2, \dots, h_2, 0) + h_1 e_0 e_0^T + h_1 e_N e_N^T \geq h_1 e_0 e_0^T + h_1 e_N e_N^T, \quad (66)$$

or, equivalently,

$$\mathbf{u}^T H_x \mathbf{u} \geq h_1 (e_0^T \mathbf{u})^2 + h_1 (e_N^T \mathbf{u})^2 \quad \forall \mathbf{u}. \quad (67)$$

4.3 Multi-dimensional first-derivative operators

Let operators with subscripts x_i denote one-dimensional operators corresponding to coordinate direction x_i . The multi-dimensional first derivatives $D_i \approx \partial_i$ are constructed using tensor products:

$$D_i = I_{x_1} \otimes I_{x_2} \otimes \cdots \otimes I_{x_{i-1}} \otimes D_{x_i} \otimes \cdots \otimes I_{x_d}, \quad (68)$$

where the I_{x_i} are one-dimensional identity matrices of appropriate sizes. In analogy with the chain rule (21), we define

$$D_{\text{I}} = F_{\text{I}i} D_i, \quad (69)$$

where $D_I \approx \partial_I$. Note that in the discrete setting, F_{Ii} is to be interpreted as a diagonal matrix holding the grid-point values of the continuous coefficient F_{Ii} for each fixed I and i . Similarly, D_i is a matrix for each fixed i . The implied summation in $F_{Ii}D_i$ hence adds matrices in $\mathbb{R}^{N \times N}$, where N denotes the total number of grid points, not elements of such matrices.

The multi-dimensional quadrature is

$$H = H_{x_1} \otimes \cdots \otimes H_{x_d}. \quad (70)$$

Let $\partial\omega_i^-$ and $\partial\omega_i^+$ denote the boundary faces where $x_i = 0$ and $x_i = 1$, respectively. For integration over boundary faces, we define

$$H_{\partial\omega_i} = H_{x_1} \otimes \cdots \otimes H_{x_{i-1}} \otimes H_{x_{i+1}} \otimes \cdots \otimes H_{x_d}. \quad (71)$$

Note that $H_{\partial\omega_i}$ can be used to integrate over $\partial\omega_i^+$ as well as $\partial\omega_i^-$. For discrete integration over the volume, we define

$$(\mathbf{u}, \mathbf{v})_\omega = \mathbf{u}^T H \mathbf{v}. \quad (72)$$

We use the same inner product notation as in the continuous case without risk of confusion since the boldface font denotes discrete solution vectors.

Let e_f^T denote a restriction operator that picks out only those solution values that reside on the face f . For discrete integration over the face $\partial\omega_i^+$, for example, we write

$$(\mathbf{u}, \mathbf{v})_{\partial\omega_i^+} = (e_{\partial\omega_i^+}^T \mathbf{u})^T H_{\partial\omega_i} (e_{\partial\omega_i^+}^T \mathbf{v}). \quad (73)$$

Let $\widehat{\partial\omega}$ denote the set of all faces of ω ,

$$\widehat{\partial\omega} = \{\partial\omega_1^-, \dots, \partial\omega_d^-, \partial\omega_1^+, \dots, \partial\omega_d^+\}. \quad (74)$$

For integration over the entire boundary $\partial\omega$, we define

$$(\mathbf{u}, \mathbf{v})_{\partial\omega} = \sum_{f \in \widehat{\partial\omega}} (\mathbf{u}, \mathbf{v})_f, \quad (75)$$

i.e., the integration is performed over one face at a time. If the integrand contains the unit normal or the scale factor \hat{J} , their values at edges and corners are defined to be the same as on the remainder of that face. In analogy with (38) and (39), we define

$$(\mathbf{u}, \mathbf{v})_\Omega = (\mathbf{u}, J \mathbf{v})_\omega \quad (76)$$

and

$$(\mathbf{u}, \mathbf{v})_{\partial\Omega} = \left(\mathbf{u}, \hat{J} \mathbf{v} \right)_{\partial\omega}. \quad (77)$$

With the notation established in this section, we have the discrete integration-by-parts formula

$$(\mathbf{u}, D_i b D_j \mathbf{v})_\omega = (\mathbf{u}, \nu_i b D_j \mathbf{v})_{\partial\omega} - (D_i \mathbf{u}, b D_j \mathbf{v})_\omega. \quad (78)$$

4.4 Multi-dimensional narrow-stencil second-derivative operators

For any fixed i , we construct

$$D_{ii}^{\text{FC}}(b) \approx \partial_i b \partial_i \quad (\text{no sum over } i), \quad (79)$$

by using the one-dimensional operator D_{xx}^{FC} for each grid line. The multi-dimensional fully compatible SBP property for the second derivative that follows is

$$(\mathbf{u}, D_{ii}^{\text{FC}}(b)\mathbf{v})_{\omega} = (\mathbf{u}, \nu_i b D_i \mathbf{v})_{\partial\omega} - (D_i \mathbf{u}, b D_i \mathbf{v})_{\omega} - \mathbf{u}^T R_{ii}(b) \mathbf{v} \quad (\text{no sum over } i), \quad (80)$$

where the R_{ii} matrices are multi-dimensional versions of R_{xx} . They inherit the symmetry and semidefiniteness-preserving properties of R_{xx} . In particular,

$$R_{ii}(b) = R_{ii}^T(b) \quad (\text{no sum over } i) \quad (81)$$

and

$$\mathbf{u}_j R_{ii}(c_{mjml}) \mathbf{u}_\ell \geq 0 \quad \forall \mathbf{u}_j \quad (\text{no sum over } i). \quad (82)$$

4.5 Multi-dimensional positivity properties

To suppress unnecessary notation, we assume that the grid spacing in the reference domain is the same in each dimension (the analysis does not rely on this assumption). It follows from (67) that (see [2])

$$(\mathbf{s}_{ij}, c_{ijkl} \mathbf{s}_{kl})_{\omega} \geq h_1 \left((\mathbf{s}_{ij}, c_{ijkl} \mathbf{s}_{kl})_{\partial\omega_m^+} + (\mathbf{s}_{ij}, c_{ijkl} \mathbf{s}_{kl})_{\partial\omega_m^-} \right), \quad (83)$$

for $m = 1, \dots, d$. Using (83) we can derive

$$\begin{aligned} (\mathbf{s}_{ij}, c_{ijkl} \mathbf{s}_{kl})_{\omega} &= \frac{1}{d} \sum_{m=1}^d (\mathbf{s}_{ij}, c_{ijkl} \mathbf{s}_{kl})_{\omega} \\ &\geq \frac{1}{d} \sum_{m=1}^d h_1 \left((\mathbf{s}_{ij}, c_{ijkl} \mathbf{s}_{kl})_{\partial\omega_m^+} + (\mathbf{s}_{ij}, c_{ijkl} \mathbf{s}_{kl})_{\partial\omega_m^-} \right) \\ &= \frac{h_1}{d} (\mathbf{s}_{ij}, c_{ijkl} \mathbf{s}_{kl})_{\partial\omega}, \end{aligned} \quad (84)$$

which we summarize as

$$(\mathbf{s}_{ij}, c_{ijkl} \mathbf{s}_{kl})_{\omega} \geq \frac{h_1}{d} (\mathbf{s}_{ij}, c_{ijkl} \mathbf{s}_{kl})_{\partial\omega}. \quad (85)$$

Using (85), we can derive a similar property for integrals in the physical domain,

$$\begin{aligned} (\mathbf{s}_{IJ}, C_{IJKL} \mathbf{s}_{KL})_{\Omega} &= (\mathbf{s}_{IJ}, JC_{IJKL} \mathbf{s}_{KL})_{\omega} \geq \frac{h_1}{d} (\mathbf{s}_{IJ}, JC_{IJKL} \mathbf{s}_{KL})_{\partial\omega} \\ &= \frac{h_1}{d} \left(\mathbf{s}_{IJ}, \hat{J}^{-1} JC_{IJKL} \mathbf{s}_{KL} \right)_{\partial\Omega}, \end{aligned} \quad (86)$$

which we summarize as

$$(\mathbf{s}_{IJ}, C_{IJKL} \mathbf{s}_{KL})_{\Omega} \geq \frac{h_1}{d} \left(\mathbf{s}_{IJ}, \hat{J}^{-1} J C_{IJKL} \mathbf{s}_{KL} \right)_{\partial\Omega}. \quad (87)$$

4.6 Combining narrow-stencil derivatives and mixed derivatives

To discretize a term such as $\partial_i b \partial_j$, using narrow-stencil second derivatives when possible, we define the operator \mathbb{D}_{ij} as

$$\mathbb{D}_{ij}(b) = \begin{cases} D_{ij}^{\text{FC}}(b), & i = j \\ D_i b D_j, & i \neq j \end{cases}. \quad (88)$$

We use blackboard bold for discrete two-tensors such as \mathbb{D}_{ij} (where each tensor element is a square matrix). Combining the two integration-by-parts formulas (78) and (80) leads to the integration-by-parts formula

$$(\mathbf{u}, \mathbb{D}_{ij}(b) \mathbf{v})_{\omega} = \begin{cases} (\mathbf{u}, \nu_i b D_j \mathbf{v})_{\partial\omega} - (D_i \mathbf{u}, b D_j \mathbf{v})_{\omega} & i \neq j \\ (\mathbf{u}, \nu_i b D_j \mathbf{v})_{\partial\omega} - (D_i \mathbf{u}, b D_j \mathbf{v})_{\omega} - \mathbf{u}^T R_{ij}(b) \mathbf{v} & i = j \end{cases}. \quad (89)$$

4.7 The discrete elastic operator

The discrete operator that approximates $\partial_i c_{ijkl} \partial_k$ is $\mathbb{D}_{ik}(c_{ijkl})$. By (89), we have

$$(\mathbf{u}_j, \mathbb{D}_{ik}(c_{ijkl}) \mathbf{v}_{\ell})_{\omega} = (\mathbf{u}_j, \nu_i c_{ijkl} D_k \mathbf{v}_{\ell})_{\partial\omega} - (D_i \mathbf{u}_j, c_{ijkl} D_k \mathbf{v}_{\ell})_{\omega} - \sum_k \mathbf{u}_j^T R_{kk}(c_{ijkl}) \mathbf{v}_{\ell}. \quad (90)$$

To simplify the notation in what follows, we define

$$\mathbb{W}_{j\ell} = \sum_k R_{kk}(c_{kjkl}). \quad (91)$$

Due to the major symmetry of c_{ijkl} (32) and the symmetry $R_{kk} = R_{kk}^T$, we have

$$\mathbb{W}_{j\ell} = \mathbb{W}_{\ell j} = \mathbb{W}_{j\ell}^T. \quad (92)$$

By (82), $\mathbb{W}_{j\ell}$ is positive semidefinite, i.e.,

$$\mathbf{u}_j^T \mathbb{W}_{j\ell} \mathbf{u}_{\ell} \geq 0 \quad \forall \mathbf{u}_j. \quad (93)$$

Another property that $\mathbb{W}_{j\ell}$ inherits from R_{xx} is that it is zero to the order of accuracy in the sense that

$$\mathbf{u}_j^T \mathbb{W}_{j\ell} \mathbf{v}_{\ell} = \mathcal{O}(h^{2q}) \quad (94)$$

for all $\mathbf{u}_j, \mathbf{v}_\ell$ that are restrictions of smooth functions to the grid. Thus, $\mathbb{W}_{j\ell}$ is a consistent approximation of the zero operator and we write $\mathbb{W}_{j\ell} \approx 0$. We restate (90) as

$$(\mathbf{u}_j, \mathbb{D}_{ik}(c_{ijkl})\mathbf{v}_\ell)_\omega = (\mathbf{u}_j, \nu_i c_{ijkl} D_k \mathbf{v}_\ell)_{\partial\omega} - (D_i \mathbf{u}_j, c_{ijkl} D_k \mathbf{v}_\ell)_\omega - \mathbf{u}_j^T \mathbb{W}_{j\ell} \mathbf{v}_\ell. \quad (95)$$

At this point, we introduce the following two new definitions, which extend the SBP concept to operators of the form $\partial_i c_{ijkl} \partial_k$.

Definition 1. Given a discrete inner product that approximates $(\cdot, \cdot)_\omega$ and a non-negative bilinear form that approximates $(\cdot, \cdot)_{\partial\omega}$, we say that $\mathbb{D}_{ik}^{\text{SBP}}(c_{ijkl})$ is an SBP operator for $\partial_i c_{ijkl} \partial_k$ on ω if

$$(\mathbf{u}_j, \mathbb{D}_{ik}^{\text{SBP}}(c_{ijkl})\mathbf{v}_\ell)_\omega = \left(\mathbf{u}_j, \nu_i c_{ijkl} \tilde{D}_k \mathbf{v}_\ell \right)_{\partial\omega} - (D_i \mathbf{u}_j, c_{ijkl} D_k \mathbf{v}_\ell)_\omega - \mathbf{u}_j^T \mathbb{W}_{j\ell} \mathbf{v}_\ell, \quad (96)$$

where $D_i \approx \partial_i$, $\tilde{D}_i \approx \partial_i$, $\mathbb{W}_{j\ell} = \mathbb{W}_{\ell j}^T \approx 0$, and $\mathbf{u}_j^T \mathbb{W}_{j\ell} \mathbf{u}_\ell \geq 0 \forall \mathbf{u}_j$.

Definition 2. An operator $\mathbb{D}_{ik}^{\text{SBP}}(c_{ijkl})$ is called a *fully compatible* SBP operator for $\partial_i c_{ijkl} \partial_k$ on ω if it satisfies (96) with $\tilde{D}_i = D_i$.

The statement (95) shows that $\mathbb{D}_{ik}(c_{ijkl})$, which was defined in (88) and is based on fully compatible one-dimensional SBP operators, is a fully compatible SBP operator for $\partial_i c_{ijkl} \partial_k$. However, Definitions 1 and 2 are intended to be more general. We anticipate that operators generated by several other stable discretization methods can be shown to be SBP operators.

The following lemma shows that an SBP operator for $\partial_i c_{ijkl} \partial_k$ also mimics the formula that follows from using integration by parts twice:

$$(u_j, \partial_i c_{ijkl} \partial_k v_\ell)_\omega = (u_j, \nu_i c_{ijkl} \partial_k v_\ell)_{\partial\omega} - (\nu_i c_{ijkl} \partial_k u_\ell, v_j)_{\partial\omega} + (\partial_i c_{ijkl} \partial_k u_\ell, v_j)_\omega. \quad (97)$$

Lemma 2. If $\mathbb{D}_{ik}^{\text{SBP}}(c_{ijkl})$ is an SBP operator for $\partial_i c_{ijkl} \partial_k$, then

$$(\mathbf{u}_j, \mathbb{D}_{ik}^{\text{SBP}}(c_{ijkl})\mathbf{v}_\ell)_\omega = \left(\mathbf{u}_j, \nu_i c_{ijkl} \tilde{D}_k \mathbf{v}_\ell \right)_{\partial\omega} - \left(\nu_i c_{ijkl} \tilde{D}_k \mathbf{u}_\ell, \mathbf{v}_j \right)_{\partial\omega} + (\mathbb{D}_{ik}^{\text{SBP}}(c_{ijkl})\mathbf{u}_\ell, \mathbf{v}_j)_\omega. \quad (98)$$

Proof. By Definition 1,

$$(\mathbf{u}_j, \mathbb{D}_{ik}^{\text{SBP}}(c_{ijkl})\mathbf{v}_\ell)_\omega = \left(\mathbf{u}_j, \nu_i c_{ijkl} \tilde{D}_k \mathbf{v}_\ell \right)_{\partial\omega} - (D_i \mathbf{u}_j, c_{ijkl} D_k \mathbf{v}_\ell)_\omega - \mathbf{u}_j^T \mathbb{W}_{j\ell} \mathbf{v}_\ell. \quad (99)$$

Using the symmetry of $(\cdot, \cdot)_\omega$ and $(\cdot, \cdot)_{\partial\omega}$, the major symmetry of c_{ijkl} (32), and $\mathbb{W}_{j\ell} = \mathbb{W}_{\ell j}^T$, we can write (99) as

$$(\mathbb{D}_{ik}^{\text{SBP}}(c_{ijkl})\mathbf{v}_\ell, \mathbf{u}_j)_\omega = \left(\nu_i c_{ijkl} \tilde{D}_k \mathbf{v}_\ell, \mathbf{u}_j \right)_{\partial\omega} - (D_i \mathbf{v}_j, c_{ijkl} D_k \mathbf{u}_\ell)_\omega - \mathbf{v}_j^T \mathbb{W}_{j\ell} \mathbf{u}_\ell. \quad (100)$$

Swapping \mathbf{u}_j and \mathbf{v}_j in (100) leads to

$$(\mathbb{D}_{ik}^{\text{SBP}}(c_{ijkl})\mathbf{u}_\ell, \mathbf{v}_j)_\omega = \left(\nu_i c_{ijkl} \tilde{D}_k \mathbf{u}_\ell, \mathbf{v}_j \right)_{\partial\omega} - (D_i \mathbf{u}_j, c_{ijkl} D_k \mathbf{v}_\ell)_\omega - \mathbf{u}_j^T \mathbb{W}_{j\ell} \mathbf{v}_\ell. \quad (101)$$

Subtracting (101) from (99) yields

$$(\mathbf{u}_j, \mathbb{D}_{ik}^{\text{SBP}}(c_{ijkl})\mathbf{v}_\ell)_\omega - (\mathbb{D}_{ik}^{\text{SBP}}(c_{ijkl})\mathbf{u}_\ell, \mathbf{v}_j)_\omega = \left(\mathbf{u}_j, \nu_i c_{ijkl} \tilde{D}_k \mathbf{v}_\ell \right)_{\partial\omega} - \left(\nu_i c_{ijkl} \tilde{D}_k \mathbf{u}_\ell, \mathbf{v}_j \right)_{\partial\omega} \quad (102)$$

and the result follows after rearranging terms. \square

We are now in position to use formula (31) to construct an FD operator that approximates $\partial_i C_{ijkl} \partial_k$. We define

$$\mathbb{D}_{ik}^\Omega(C_{ijkl}) := J^{-1} \mathbb{D}_{ik}(c_{ijkl}). \quad (103)$$

The main result of this section is stated in the following theorem.

Theorem 1. *The operator $\mathbb{D}_{ik}^\Omega(C_{ijkl}) = J^{-1} \mathbb{D}_{ik}(c_{ijkl})$ is a fully compatible SBP operator for $\partial_i C_{ijkl} \partial_k$ on the physical domain Ω .*

Proof. We first derive a formula that simplifies the proof of the theorem. Using first the definition of c_{ijkl} and then Nanson's formula (42), we obtain

$$\nu_i c_{ijkl} = \nu_i F_{ii} J C_{ijkl} F_{kk} = J^{-1} \hat{J} n_i J C_{ijkl} F_{kk} = \hat{J} n_i C_{ijkl} F_{kk}. \quad (104)$$

We are now ready to prove the result. We have

$$\begin{aligned} (\mathbf{u}_j, \mathbb{D}_{ik}^\Omega(C_{ijkl})\mathbf{v}_L)_\Omega &= (\mathbf{u}_j, J^{-1} \mathbb{D}_{ik}(c_{ijkl})\mathbf{v}_L)_\Omega \\ &= (\mathbf{u}_j, \mathbb{D}_{ik}(c_{ijkl})\mathbf{v}_L)_\omega \quad [\text{Use (95)}] \\ &= (\mathbf{u}_j, \nu_i c_{ijkl} D_k \mathbf{v}_L)_{\partial\omega} - (D_i \mathbf{u}_j, c_{ijkl} D_k \mathbf{v}_L)_\omega - \mathbf{u}_j^T \mathbb{W}_{jL} \mathbf{v}_L \quad [\text{Use (104)}] \\ &= \left(\mathbf{u}_j, \hat{J} n_i C_{ijkl} F_{kk} D_k \mathbf{v}_L \right)_{\partial\omega} - (D_i \mathbf{u}_j, F_{ii} J C_{ijkl} F_{kk} D_k \mathbf{v}_L)_\omega \\ &\quad - \mathbf{u}_j^T \mathbb{W}_{jL} \mathbf{v}_L \\ &= (\mathbf{u}_j, n_i C_{ijkl} D_k \mathbf{v}_L)_{\partial\Omega} - (D_i \mathbf{u}_j, C_{ijkl} D_k \mathbf{v}_L)_\Omega - \mathbf{u}_j^T \mathbb{W}_{jL} \mathbf{v}_L. \end{aligned} \quad (105)$$

\square

In analogy with the continuous traction operator T_{JL} defined in (13), we define the discrete traction operator

$$\mathbb{T}_{JL} = n_I C_{IJKL} D_K. \quad (106)$$

The integration-by-parts formulas satisfied by $\mathbb{D}_{IK}^\Omega(C_{IJKL})$ now read

$$\begin{aligned} (\mathbf{u}_J, \mathbb{D}_{IK}^\Omega(C_{IJKL})\mathbf{v}_L)_\Omega &= (\mathbf{u}_J, \mathbb{T}_{JL}\mathbf{v}_L)_{\partial\Omega} - (D_I \mathbf{u}_J, C_{IJKL} D_K \mathbf{v}_L)_\Omega \\ &\quad - \mathbf{u}_J^T \mathbb{W}_{JL} \mathbf{v}_L \end{aligned} \quad (107)$$

and

$$\begin{aligned} (\mathbf{u}_J, \mathbb{D}_{IK}^\Omega(C_{IJKL})\mathbf{v}_L)_\Omega &= (\mathbf{u}_J, \mathbb{T}_{JL}\mathbf{v}_L)_{\partial\Omega} - (\mathbb{T}_{JL}\mathbf{u}_L, \mathbf{v}_J)_{\partial\Omega} \\ &\quad + (\mathbb{D}_{IK}^\Omega(C_{IJKL})\mathbf{u}_L, \mathbf{v}_J)_\Omega. \end{aligned} \quad (108)$$

5 Energy-stable and self-adjoint boundary SATs

We discretize the problem (11) in space as

$$\rho \ddot{\mathbf{u}}_J = \mathbb{D}_{IK}^\Omega(C_{IJKL})\mathbf{u}_L + \mathbf{f}_J + SAT_J, \quad (109)$$

where the SATs in SAT_J impose the boundary conditions and will be specified later. For notational convenience we assume $f_J = 0$ in the following analysis. Multiplying (109) by $\phi_J^T JH$, where ϕ_J is an arbitrary test function, leads to the equivalent weak form:

$$(\phi_J, \rho \ddot{\mathbf{u}}_J)_\Omega = (\phi_J, \mathbb{D}_{IK}^\Omega(C_{IJKL})\mathbf{u}_L)_\Omega + (\phi_J, SAT_J)_\Omega. \quad (110)$$

After using the integration-by-parts formula (107), the weak form reads

$$\begin{aligned} (\phi_J, \rho \ddot{\mathbf{u}}_J)_\Omega &= (\phi_J, \mathbb{T}_{JL}\mathbf{u}_L)_{\partial\Omega} - (D_I \phi_J, C_{IJKL} D_K \mathbf{u}_L)_\Omega - \phi_J^T \mathbb{W}_{JL} \mathbf{u}_L \\ &\quad + (\phi_J, SAT_J)_\Omega. \end{aligned} \quad (111)$$

Define the inner product

$$M(\vec{\phi}, \vec{\mathbf{u}}) = (\phi_J, \rho \mathbf{u}_J)_\Omega, \quad (112)$$

the symmetric positive semidefinite bilinear form

$$K(\vec{\phi}, \vec{\mathbf{u}}) = (D_I \phi_J, C_{IJKL} D_K \mathbf{u}_L)_\Omega + \phi_J^T \mathbb{W}_{JL} \mathbf{u}_L, \quad (113)$$

and

$$B(\vec{\phi}, \vec{\mathbf{u}}) = (\phi_J, \mathbb{T}_{JL}\mathbf{u}_L)_{\partial\Omega} + (\phi_J, SAT_J)_\Omega. \quad (114)$$

In this paper SAT_J is always linear in $\vec{\mathbf{u}}$ and thus $B(\cdot, \cdot)$ is a bilinear form in the case of homogeneous boundary conditions. The weak form can now be written as

$$M(\vec{\phi}, \vec{\mathbf{u}}) + K(\vec{\phi}, \vec{\mathbf{u}}) = B(\vec{\phi}, \vec{\mathbf{u}}). \quad (115)$$

We define the discrete energy

$$\begin{aligned} E &:= \frac{1}{2} (\dot{\mathbf{u}}_J, \rho \dot{\mathbf{u}}_J)_\Omega + \frac{1}{2} (D_I \mathbf{u}_J, C_{IJKL} D_K \mathbf{u}_L)_\Omega + \frac{1}{2} \mathbf{u}_J^T \mathbb{W}_{JL} \mathbf{u}_L \\ &= \frac{1}{2} M(\dot{\mathbf{u}}, \dot{\mathbf{u}}) + \frac{1}{2} K(\mathbf{u}, \mathbf{u}). \end{aligned} \quad (116)$$

Recalling that \mathbb{W}_{JL} is zero to order $2q$, we conclude that the discrete energy E approximates the continuous energy \mathcal{E} defined in (17). It follows from the non-negativity of M and K that E is a non-negative quantity. Setting $\vec{\phi} = \dot{\mathbf{u}}$ in (115) yields the discrete energy rate

$$\frac{dE}{dt} = B(\dot{\mathbf{u}}, \dot{\mathbf{u}}). \quad (117)$$

For future use we note that the integration-by-parts formula (107) can be written as

$$(\phi_J, \mathbb{D}_{IK}^\Omega (C_{IJKL}) \mathbf{u}_L)_\Omega = (\phi_J, \mathbb{T}_{JL} \mathbf{u}_L)_{\partial\Omega} - K(\vec{\phi}, \vec{\mathbf{u}}). \quad (118)$$

5.1 Robin boundary conditions

Consider Robin boundary conditions,

$$T_{JL} u_L + U_{JL} u_L = g_J, \quad \vec{X} \in \partial\Omega, \quad (119)$$

where $U_{JL} = U_{LJ}$ and $u_J U_{JL} u_L \geq 0 \ \forall u_J$. Robin conditions include the important case of traction conditions, obtained by setting $U_{JL} = 0$ in (119). It follows from (18) that, for $g_J = 0$, the continuous solution satisfies the energy balance

$$\frac{d\tilde{\mathcal{E}}}{dt} = 0, \quad (120)$$

where

$$\tilde{\mathcal{E}} = \mathcal{E} + \frac{1}{2} (u_J, U_{JL} u_L)_{\partial\Omega}. \quad (121)$$

If SAT_J satisfies

$$(\phi_J, SAT_J)_\Omega = -(\phi_J, \mathbb{T}_{JL} \mathbf{u}_L + U_{JL} \mathbf{u}_L - g_J)_{\partial\Omega}, \quad (122)$$

then, for $g_J = 0$, we obtain

$$\begin{aligned} B(\vec{\phi}, \vec{\mathbf{u}}) &= (\phi_J, \mathbb{T}_{JL} \mathbf{u}_L)_{\partial\Omega} - (\phi_J, \mathbb{T}_{JL} \mathbf{u}_L + U_{JL} \mathbf{u}_L)_{\partial\Omega} \\ &= -(\phi_J, U_{JL} \mathbf{u}_L)_{\partial\Omega}, \end{aligned} \quad (123)$$

which is a symmetric bilinear form. It follows that

$$B(\dot{\mathbf{u}}, \dot{\mathbf{u}}) = -\frac{1}{2} \frac{d}{dt} (\mathbf{u}_J, U_{JL} \mathbf{u}_L)_{\partial\Omega}, \quad (124)$$

which yields the energy balance

$$\frac{d}{dt} \tilde{E} = 0, \quad (125)$$

where

$$\tilde{E} = E + \frac{1}{2} (\mathbf{u}_J, U_{JL} \mathbf{u}_L)_{\partial\Omega} \geq 0, \quad (126)$$

which shows that the scheme is energy stable. We achieve (122) by setting

$$SAT_J = -(JH)^{-1} \sum_{f \in \widehat{\partial\omega}} e_f \hat{J} H_f (e_f^T (\mathbb{T}_{JL} \mathbf{u}_L + U_{JL} \mathbf{u}_L) - \mathbf{g}_J), \quad (127)$$

where $\widehat{\partial\omega}$ denotes the set of all faces and was defined in (74). The SAT (127) is the standard SAT for Robin boundary conditions, see [14].

Remark 1. Robin boundary conditions can be generalized by introducing an additional term $V_{JL} \dot{u}_L$, where $u_J V_{JL} u_L \geq 0 \forall u_J$, on the left-hand side of (119). This term introduces energy dissipation in the continuous problem. It is straightforward to generalize the SAT (122) to such BC and obtain corresponding dissipation of discrete energy, see [14]. To streamline the discussion of self-adjointness, however, we restrict our attention to Robin and displacement conditions in this paper.

5.2 Displacement boundary conditions

We now consider displacement conditions,

$$u_J = g_J, \quad \vec{X} \in \partial\Omega. \quad (128)$$

The homogeneous conditions obtained by setting $g_J = 0$ are energy-conserving for the continuous equations. However, there are no consistent SATs that make $B(\vec{\phi}, \vec{u})$ vanish. Instead, we shall choose SATs that symmetrize the form $B(\cdot, \cdot)$. Suppose that

$$(\phi_J, SAT_J)_\Omega = (\mathbb{T}_{LJ} \phi_J, \mathbf{u}_L - \mathbf{g}_L)_{\partial\Omega} - (\mathbb{Z}_{LJ} \phi_J, \mathbf{u}_L - \mathbf{g}_L)_{\partial\Omega}, \quad (129)$$

for some yet unspecified \mathbb{Z}_{JL} that is symmetric with respect to the boundary quadrature in the sense that

$$(\mathbb{Z}_{LJ} \cdot, \cdot)_{\partial\Omega} = (\cdot, \mathbb{Z}_{JL} \cdot)_{\partial\Omega}. \quad (130)$$

Then, for $g_J = 0$, we obtain

$$B(\vec{\phi}, \vec{u}) = (\phi_J, \mathbb{T}_{JL} \mathbf{u}_L)_{\partial\Omega} + (\mathbb{T}_{LJ} \phi_J, \mathbf{u}_L)_{\partial\Omega} - (\phi_J, \mathbb{Z}_{JL} \mathbf{u}_L)_{\partial\Omega}, \quad (131)$$

which is a symmetric bilinear form. It follows that

$$\frac{dE}{dt} = B(\dot{\vec{u}}, \vec{u}) = \frac{1}{2} \frac{d}{dt} B(\vec{u}, \vec{u}). \quad (132)$$

We obtain the energy balance

$$\frac{dE_d}{dt} = 0, \quad (133)$$

where the modified energy E_d is

$$E_d = E - \frac{1}{2}B(\vec{\mathbf{u}}, \vec{\mathbf{u}}) = E - (\mathbf{u}_J, \mathbb{T}_{JL}\mathbf{u}_L)_{\partial\Omega} + \frac{1}{2}(\mathbf{u}_J, \mathbb{Z}_{JL}\mathbf{u}_L)_{\partial\Omega}. \quad (134)$$

Note that E_d , just like E , is a high-order approximation of the continuous energy \mathcal{E} because $B(\vec{\mathbf{u}}, \vec{\mathbf{u}})$ is zero to the order of accuracy due to the boundary condition.

The SAT that satisfies (129) is

$$SAT_J = (JH)^{-1} \sum_{f \in \widehat{\partial\omega}} (\mathbb{T}_{LJ} - \mathbb{Z}_{LJ})^T e_f \hat{H}_f (e_f^T \mathbf{u}_L - \mathbf{g}_L), \quad (135)$$

where \mathbb{Z}_{LJ} remains unspecified at this point. The ansatz (135) ensures that the SATs are consistent with displacement boundary conditions. For fixed J and L , \mathbb{Z}_{LJ} is an $N \times N$ matrix with units of force per unit volume. For SAT_J to have the same h -dependence as $\mathbb{D}_{IK}^\Omega(C_{IJKL})$, which is a second derivative and hence scales as h^{-2} , the entries of \mathbb{Z}_{LJ} must be proportional to h^{-1} . Because the boundary quadrature operator is diagonal, the condition (130) is satisfied if $\mathbb{Z}_{JL} = \mathbb{Z}_{LJ}$ and \mathbb{Z}_{JL} is diagonal for each J and L .

To prove stability, it remains to prove that we can choose \mathbb{Z}_{LJ} so that E_d is a non-negative quantity. To accomplish this, we use the positivity of E . Since the indefinite term in E_d is a surface integral, we bound E from below by a surface integral. We have

$$\begin{aligned} 2E &= (\dot{\mathbf{u}}_J, \rho \ddot{\mathbf{u}}_J)_\Omega + (D_I \mathbf{u}_J, C_{IJKL} D_K \mathbf{u}_L)_\Omega + \mathbf{u}_J^T \mathbb{W}_{JL} \mathbf{u}_L \\ &\geq \frac{h_1}{d} \left(D_I \mathbf{u}_J, \frac{J}{\hat{J}} C_{IJKL} D_K \mathbf{u}_L \right)_{\partial\Omega}, \end{aligned} \quad (136)$$

where we used the positivity property (87) in the last step. Using (136) in (134) yields

$$\begin{aligned} 2E_d &\geq \frac{h_1}{d} \left(D_I \mathbf{u}_J, \hat{J}^{-1} J C_{IJKL} D_K \mathbf{u}_L \right)_{\partial\Omega} - 2(\mathbf{u}_J, \mathbb{T}_{JL} \mathbf{u}_L)_{\partial\Omega} \\ &\quad + (\mathbf{u}_J, \mathbb{Z}_{JL} \mathbf{u}_L)_{\partial\Omega}. \end{aligned} \quad (137)$$

Recalling the definition of \mathbb{T}_{JL} (106) lets us write

$$(\mathbf{u}_J, \mathbb{T}_{JL} \mathbf{u}_L)_{\partial\Omega} = (\mathbf{u}_J, n_I C_{IJKL} D_K \mathbf{u}_L)_{\partial\Omega} = (n_I \mathbf{u}_J, C_{IJKL} D_K \mathbf{u}_L)_{\partial\Omega}. \quad (138)$$

Due to the major symmetry of C_{IJKL} (32), we have

$$(n_I \mathbf{u}_J, C_{IJKL} D_K \mathbf{u}_L)_{\partial\Omega} = (n_K \mathbf{u}_L, C_{IJKL} D_I \mathbf{u}_J)_{\partial\Omega}. \quad (139)$$

By completing the squares, we obtain

$$\begin{aligned}
2E_d &\geq \frac{h_1}{d} \left(D_I \mathbf{u}_J, \hat{J}^{-1} J C_{IJKL} D_K \mathbf{u}_L \right)_{\partial\Omega} - 2 (n_I \mathbf{u}_J, C_{IJKL} D_K \mathbf{u}_L)_{\partial\Omega} \\
&\quad + (\mathbf{u}_J, \mathbb{Z}_{JL} \mathbf{u}_L)_{\partial\Omega} \\
&= \frac{h_1}{d} \left(D_I \mathbf{u}_J - \frac{d\hat{J}}{h_1 J} n_I \mathbf{u}_J, \frac{J}{\hat{J}} C_{IJKL} \left(D_K \mathbf{u}_L - \frac{d\hat{J}}{h_1 J} n_K \mathbf{u}_L \right) \right)_{\partial\Omega} \quad (140) \\
&\quad - \left(n_I \mathbf{u}_J, \frac{d\hat{J}}{h_1 J} C_{IJKL} n_K \mathbf{u}_L \right)_{\partial\Omega} + (\mathbf{u}_J, \mathbb{Z}_{JL} \mathbf{u}_L)_{\partial\Omega} \\
&\geq \left(\mathbf{u}_J, \left(\mathbb{Z}_{JL} - \frac{d\hat{J}}{h_1 J} n_I C_{IJKL} n_K \right) \mathbf{u}_L \right)_{\partial\Omega}.
\end{aligned}$$

We achieve $E_d \geq 0$ by setting

$$\mathbb{Z}_{JL} = \beta \frac{d\hat{J}}{h_1 J} n_I C_{IJKL} n_K, \quad \beta \geq 1. \quad (141)$$

Since \hat{J} , J , n_I , and C_{IJKL} are diagonal matrices in the discrete case, the \mathbb{Z}_{JL} are diagonal matrices. Using the major symmetry of C_{IJKL} (7), we have

$$\mathbb{Z}_{JL} = \beta \frac{d\hat{J}}{h_1 J} n_I C_{IJKL} n_K = \beta \frac{d\hat{J}}{h_1 J} n_I C_{KLIJ} n_K = \mathbb{Z}_{LJ}, \quad (142)$$

which verifies that \mathbb{Z}_{JL} satisfies the symmetry assumption (130). We have now proven the following theorem.

Theorem 2. *The scheme*

$$\rho \ddot{\mathbf{u}}_J = \mathbb{D}_{IK}^\Omega (C_{IJKL}) \mathbf{u}_L + (JH)^{-1} \sum_{f \in \widehat{\partial\omega}} (\mathbb{T}_{LJ} - \mathbb{Z}_{LJ})^T e_f \hat{J} H_f (e_f^T \mathbf{u}_L - \mathbf{g}_L), \quad (143)$$

with

$$\mathbb{Z}_{JL} = \beta \frac{d\hat{J}}{h_1 J} n_I C_{IJKL} n_K \quad (144)$$

is stable if $\beta \geq 1$.

In all simulations in this paper, we set $\beta = 1$, i.e., right on the limit of provable stability. The drawback of using larger values of β is that this increases the spectral radius of the operator.

5.3 Self-adjointness

The adjoint of the discrete operator plays an important role in PDE-constrained optimization problems such as seismic imaging, where the adjoint state

method is frequently used to compute the gradient of the objective functional. The continuous elastic operator is self-adjoint, and this subsection is devoted to proving that the discrete elastic operator is also self-adjoint. A consequence of this property is that one may use the same solver for the forward and adjoint PDEs and still obtain the exact (up to roundoff error) gradient of a discrete objective functional (provided that the time-discretization is also adjoint-consistent).

Let \mathcal{U} and Φ be subsets of $L^2(\Omega)$. We think of \mathcal{U} as the primal space and Φ as the dual or adjoint space. The adjoint $\mathcal{L}_{\text{JL}}^\dagger : \Phi \rightarrow L^2(\Omega)$ of a linear operator $\mathcal{L}_{\text{JL}} : \mathcal{U} \rightarrow L^2(\Omega)$ satisfies

$$(\phi_J, \mathcal{L}_{\text{JL}} u_L)_\Omega = \left(\mathcal{L}_{\text{JL}}^\dagger \phi_L, u_J \right)_\Omega \quad \forall u_J \in \mathcal{U}, \phi_J \in \Phi. \quad (145)$$

The operator \mathcal{L}_{JL} is said to be self-adjoint if $\mathcal{L}_{\text{JL}}^\dagger = \mathcal{L}_{\text{JL}}$, which implies that $\Phi = \mathcal{U}$ [43].

We here consider the elastic operator $\mathcal{D}_{\text{JL}} = \partial_I C_{IJKL} \partial_K$. For now, we leave the domain of \mathcal{D}_{JL} unspecified. We define the space of admissible functions

$$\mathcal{U} = \{u_J \in L^2(\Omega) \mid \mathcal{D}_{\text{JL}} u_L \in L^2(\Omega)\}. \quad (146)$$

We further assume that u_J satisfies either Robin boundary conditions (119) or displacement boundary conditions (128). Let \mathcal{U}_R and \mathcal{U}_D denote the corresponding spaces:

$$\begin{aligned} \mathcal{U}_R &= \{u_J \in \mathcal{U} \mid T_{\text{JL}} u_L + U_{\text{JL}} u_L = 0 \text{ on } \partial\Omega\}, \\ \mathcal{U}_D &= \{u_J \in \mathcal{U} \mid u_J = 0 \text{ on } \partial\Omega\}. \end{aligned} \quad (147)$$

Two partial integrations yield (cf. (97))

$$(\phi_J, \mathcal{D}_{\text{JL}} u_L)_\Omega = (\phi_J, T_{\text{JL}} u_L)_{\partial\Omega} - (T_{\text{LJ}} \phi_J, u_L)_{\partial\Omega} + (\mathcal{D}_{\text{JL}} \phi_L, u_J)_\Omega. \quad (148)$$

It follows that

$$(\phi_J, \mathcal{D}_{\text{JL}} u_L)_\Omega = (\mathcal{D}_{\text{JL}} \phi_L, u_J)_\Omega \quad \forall u_J \in \mathcal{U}_R, \phi_J \in \mathcal{U}_R \quad (149)$$

and

$$(\phi_J, \mathcal{D}_{\text{JL}} u_L)_\Omega = (\mathcal{D}_{\text{JL}} \phi_L, u_J)_\Omega \quad \forall u_J \in \mathcal{U}_D, \phi_J \in \mathcal{U}_D, \quad (150)$$

which shows that \mathcal{D}_{JL} is self-adjoint both with domain \mathcal{U}_R (Robin conditions) and with domain \mathcal{U}_D (displacement conditions).

We now consider the total discrete elastic operator, including SATs for Robin or displacement boundary conditions. Assuming homogeneous boundary conditions, we can define \mathbb{S}_{JL} such that

$$SAT_J = \mathbb{S}_{\text{JL}} \mathbf{u}_L, \quad (151)$$

and the total discrete elastic operator is

$$\mathbb{D}_{\text{JL}}^{tot} = \mathbb{D}_{\text{IK}}^\Omega(C_{IJKL}) + \mathbb{S}_{\text{JL}}. \quad (152)$$

Theorem 3. *The total discrete elastic operator, including SATs for Robin or displacement boundary conditions, is self-adjoint, i.e.,*

$$(\phi_J, \mathbb{D}_{JL}^{tot} \mathbf{u}_L)_{\Omega} = (\mathbb{D}_{JL}^{tot} \phi_L, \mathbf{u}_J)_{\Omega} \quad \forall \phi_J, \mathbf{u}_J. \quad (153)$$

Proof. In deriving the weak form (115), we showed that

$$(\phi_J, \mathbb{D}_{JL}^{tot} \mathbf{u}_L)_{\Omega} = -K(\vec{\phi}, \vec{\mathbf{u}}) + B(\vec{\phi}, \vec{\mathbf{u}}), \quad (154)$$

where K is symmetric and B is symmetric both in the case of Robin conditions (cf. (123)) and in the case of displacement conditions (cf. (131)). Hence, we have

$$\begin{aligned} (\phi_J, \mathbb{D}_{JL}^{tot} \mathbf{u}_L)_{\Omega} &= -K(\vec{\phi}, \vec{\mathbf{u}}) + B(\vec{\phi}, \vec{\mathbf{u}}) = -K(\vec{\mathbf{u}}, \vec{\phi}) + B(\vec{\mathbf{u}}, \vec{\phi}) \\ &= (\mathbf{u}_J, \mathbb{D}_{JL}^{tot} \phi_L)_{\Omega}. \end{aligned} \quad (155)$$

After using the symmetry of $(\cdot, \cdot)_{\Omega}$, the result follows. \square

6 Energy-stable and self-adjoint interface SATs

We may want to introduce multiple grid blocks to: handle discontinuous material parameters ρ and C_{ijkl} , facilitate grid generation, or model earthquakes or fractures, in which case there are prescribed discontinuities in either displacement or traction. The discussion below covers all cases. The Jacobian J and transformation gradient F_{li} may be discontinuous across the interface.

Let Γ denote the interface between two domains Ω_u and Ω_v . We use superscripts u and v to distinguish between quantities that correspond to the two different sides of the interface. We consider the problem

$$\begin{aligned} \rho^u \ddot{u}_J &= \partial_i C_{ijkl}^u \partial_k u_L, \quad \vec{X} \in \Omega_u, \\ \rho^v \ddot{v}_J &= \partial_i C_{ijkl}^v \partial_k v_L, \quad \vec{X} \in \Omega_v, \\ u_J - v_J &= V_J, \quad \vec{X} \in \Gamma, \\ \tau_J^u + \tau_J^v &= \Theta_J, \quad \vec{X} \in \Gamma. \end{aligned} \quad (156)$$

augmented with suitable boundary conditions. The functions V_J and Θ_J denote data for jumps in displacement and traction, respectively. Define the energies

$$\begin{aligned} \mathcal{E}_u &= \frac{1}{2} (\dot{u}_J, \rho^u \dot{u}_J)_{\Omega_u} + \frac{1}{2} (\partial_i u_J, C_{ijkl}^u \partial_k u_L)_{\Omega_u}, \\ \mathcal{E}_v &= \frac{1}{2} (\dot{v}_J, \rho^v \dot{v}_J)_{\Omega_v} + \frac{1}{2} (\partial_i v_J, C_{ijkl}^v \partial_k v_L)_{\Omega_v}. \end{aligned} \quad (157)$$

Assuming energy-conserving boundary conditions and $V_J = \Theta_J = 0$, the energy method yields

$$\frac{d}{dt} (\mathcal{E}_u + \mathcal{E}_v) = (\dot{u}_J, \tau_J^u)_{\Gamma} + (\dot{v}_J, \tau_J^v)_{\Gamma} = 0. \quad (158)$$

We assume that the surface Jacobian \hat{J} is the same on the two sides of the interface so that grid points that coincide in the reference domain coincide also in the physical domain. In the following equations, we suppress superscripts u and v on the interface restriction operators e_Γ , because it is clear from context that, for example, $e_\Gamma^T \mathbf{u}_K$ denotes $(e_\Gamma^u)^T \mathbf{u}_K$.

We discretize (156) as

$$\begin{aligned} \rho^u \ddot{\mathbf{u}}_J &= \mathbb{D}_{IK}^{\Omega_u} (C_{IJKL}^u) \mathbf{u}_L \\ &\quad - (J^u H^u)^{-1} \mathbb{Z}_{LJ}^T e_\Gamma \hat{J} H_\Gamma (e_\Gamma^T \mathbf{u}_L - e_\Gamma^T \mathbf{v}_L - \mathbf{V}_L) \\ &\quad + \frac{1}{2} (J^u H^u)^{-1} (\mathbb{T}_{LJ}^u)^T e_\Gamma \hat{J} H_\Gamma (e_\Gamma^T \mathbf{u}_L - e_\Gamma^T \mathbf{v}_L - \mathbf{V}_L) \\ &\quad - \frac{1}{2} (J^u H^u)^{-1} e_\Gamma \hat{J} H_\Gamma (e_\Gamma^T \mathbb{T}_{JL}^u \mathbf{u}_L + e_\Gamma^T \mathbb{T}_{JL}^u \mathbf{v}_L - \Theta_J), \end{aligned} \quad (159)$$

$$\begin{aligned} \rho^v \ddot{\mathbf{v}}_J &= \mathbb{D}_{IK}^{\Omega_v} (C_{IJKL}^v) \mathbf{v}_L \\ &\quad - (J^v H^v)^{-1} \mathbb{Z}_{LJ}^T e_\Gamma \hat{J} H_\Gamma (e_\Gamma^T \mathbf{v}_L - e_\Gamma^T \mathbf{u}_L + \mathbf{V}_L) \\ &\quad + \frac{1}{2} (J^v H^v)^{-1} (\mathbb{T}_{LJ}^v)^T e_\Gamma \hat{J} H_\Gamma (e_\Gamma^T \mathbf{v}_L - e_\Gamma^T \mathbf{u}_L + \mathbf{V}_L) \\ &\quad - \frac{1}{2} (J^v H^v)^{-1} e_\Gamma \hat{J} H_\Gamma (e_\Gamma^T \mathbb{T}_{JL}^v \mathbf{v}_L + e_\Gamma^T \mathbb{T}_{JL}^v \mathbf{u}_L - \Theta_J), \end{aligned}$$

where

$$\mathbb{Z}_{JL} = \beta \frac{d}{4h_1} \hat{J} \left(\frac{n_I^u C_{IJKL}^u n_K^u}{J^u} + \frac{n_I^v C_{IJKL}^v n_K^v}{J^v} \right), \quad \beta \geq 1. \quad (160)$$

Note that \mathbb{Z}_{JL} satisfies $(\mathbb{Z}_{LJ} \cdot, \cdot)_\Gamma = (\cdot, \mathbb{Z}_{JL})_\Gamma$. The remainder of this section is devoted to proving that the scheme (159) is energy stable and self-adjoint.

To derive the weak form of (159), we multiply the first equation by $\phi_J^T J^u H^u$, which, with $\mathbf{V}_J = \Theta_J = 0$ for convenience, yields

$$\begin{aligned} (\phi_J, \rho^u \ddot{\mathbf{u}}_J)_{\Omega_u} &= (\phi_J, \mathbb{D}_{IK}^{\Omega_u} (C_{IJKL}^u) \mathbf{u}_L)_{\Omega_u} - (\mathbb{Z}_{LJ} \phi_J, \mathbf{u}_L - \mathbf{v}_L)_\Gamma \\ &\quad + \frac{1}{2} (\mathbb{T}_{LJ}^u \phi_J, \mathbf{u}_L - \mathbf{v}_L)_\Gamma - \frac{1}{2} (\phi_J, \mathbb{T}_{JL}^u \mathbf{u}_L + \mathbb{T}_{JL}^u \mathbf{v}_L)_\Gamma. \end{aligned} \quad (161)$$

Let

$$\begin{aligned} M_u(\vec{\phi}, \vec{\mathbf{u}}) &= (\phi_J, \rho^u \mathbf{u}_J)_{\Omega_u}, \\ K_u(\vec{\phi}, \vec{\mathbf{u}}) &= (D_I \phi_J, C_{IJKL}^u D_K \mathbf{u}_L)_{\Omega_u} + \phi_J^T \mathbb{W}_{JL}^u \mathbf{u}_L, \\ E_u &= \frac{1}{2} M_u(\vec{\mathbf{u}}, \vec{\mathbf{u}}) + \frac{1}{2} K_u(\vec{\mathbf{u}}, \vec{\mathbf{u}}), \end{aligned} \quad (162)$$

and define M_v , K_v , and E_v analogously. Using the integration-by-parts formula (118) in (161) yields

$$\begin{aligned} M_u(\vec{\phi}, \vec{\mathbf{u}}) + K_u(\vec{\phi}, \vec{\mathbf{u}}) &= - (\mathbb{Z}_{LJ} \phi_J, \mathbf{u}_L - \mathbf{v}_L)_\Gamma + \frac{1}{2} (\mathbb{T}_{LJ}^u \phi_J, \mathbf{u}_L - \mathbf{v}_L)_\Gamma \\ &\quad + \frac{1}{2} (\phi_J, \mathbb{T}_{JL}^u \mathbf{u}_L - \mathbb{T}_{JL}^u \mathbf{v}_L)_\Gamma. \end{aligned} \quad (163)$$

Multiplying the second equation in (159) by $\chi_J^T J^v H^v$ similarly leads to

$$\begin{aligned} M_v(\vec{\chi}, \ddot{\vec{v}}) + K_v(\vec{\chi}, \vec{v}) &= -(\mathbb{Z}_{LJ} \chi_J, \mathbf{v}_L - \mathbf{u}_L)_\Gamma + \frac{1}{2} (\mathbb{T}_{LJ}^v \chi_J, \mathbf{v}_L - \mathbf{u}_L)_\Gamma \\ &\quad + \frac{1}{2} (\chi_J, \mathbb{T}_{JL}^v \mathbf{v}_L - \mathbb{T}_{JL}^u \mathbf{u}_L)_\Gamma. \end{aligned} \quad (164)$$

We add (163) and (164) to obtain

$$M_u(\vec{\phi}, \ddot{\vec{u}}) + K_u(\vec{\phi}, \vec{u}) + M_v(\vec{\chi}, \ddot{\vec{v}}) + K_v(\vec{\chi}, \vec{v}) = I(\vec{\phi}, \vec{u}, \vec{\chi}, \vec{v}), \quad (165)$$

where I is the sum of interface integrals,

$$\begin{aligned} I(\vec{\phi}, \vec{u}, \vec{\chi}, \vec{v}) &= -(\phi_J - \chi_J, \mathbb{Z}_{JL}(\mathbf{u}_L - \mathbf{v}_L))_\Gamma \\ &\quad + \frac{1}{2} (\mathbb{T}_{JL}^u \phi_L - \mathbb{T}_{JL}^v \chi_L, \mathbf{u}_J - \mathbf{v}_J)_\Gamma \\ &\quad + \frac{1}{2} (\phi_J - \chi_J, \mathbb{T}_{JL}^u \mathbf{u}_L - \mathbb{T}_{JL}^v \mathbf{v}_L)_\Gamma. \end{aligned} \quad (166)$$

Note that I is symmetric with respect to trial and test functions in the sense that

$$I(\vec{\phi}, \vec{u}, \vec{\chi}, \vec{v}) = I(\vec{u}, \vec{\phi}, \vec{v}, \vec{\chi}). \quad (167)$$

Setting $\vec{\phi} = \dot{\vec{u}}$ and $\vec{\chi} = \dot{\vec{v}}$ yields the energy rate

$$\frac{d}{dt} (E_u + E_v) = I(\dot{\vec{u}}, \vec{u}, \dot{\vec{v}}, \vec{v}) = \frac{1}{2} \frac{d}{dt} I(\vec{u}, \vec{u}, \vec{v}, \vec{v}). \quad (168)$$

We define the discrete energy

$$\begin{aligned} E_I &= E_u + E_v - \frac{1}{2} I(\vec{u}, \vec{u}, \vec{v}, \vec{v}) \\ &= E_u + E_v + \frac{1}{2} (\mathbf{u}_J - \mathbf{v}_J, \mathbb{Z}_{JL}(\mathbf{u}_L - \mathbf{v}_L))_\Gamma - (\mathbf{u}_J - \mathbf{v}_J, \mathbb{T}_{JL}^u \mathbf{u}_L - \mathbb{T}_{JL}^v \mathbf{v}_L)_\Gamma, \end{aligned} \quad (169)$$

which satisfies

$$\frac{dE_I}{dt} = 0. \quad (170)$$

Note that E_I , just like $E_u + E_v$, approximates $\mathcal{E}_u + \mathcal{E}_v$, because the surface integrals in I would be zero if the interface conditions were fulfilled exactly.

Theorem 4. *The scheme (159) is stable.*

Proof. We have shown that the scheme conserves the discrete energy E_I . It remains to prove that E_I is a non-negative quantity. To keep the notation concise in the following, let

$$[\![\mathbf{u}]\!]_J = \mathbf{u}_J - \mathbf{v}_J \quad (171)$$

denote the jump in displacement. We can now write

$$-\frac{1}{2}I(\vec{\mathbf{u}}, \vec{\mathbf{u}}, \vec{\mathbf{v}}, \vec{\mathbf{v}}) = \frac{1}{2}(\llbracket \mathbf{u} \rrbracket_J, \mathbb{Z}_{JL} \llbracket \mathbf{u} \rrbracket_L)_\Gamma - (\llbracket \mathbf{u} \rrbracket_J, \mathbb{T}_{JL}^u \mathbf{u}_L - \mathbb{T}_{JL}^v \mathbf{v}_L)_\Gamma. \quad (172)$$

The positivity property (87) yields (cf. (136))

$$\begin{aligned} 2E_u &\geq \frac{h_1}{d} \left(D_I \mathbf{u}_J, \hat{J}^{-1} J^u C_{IJKL}^u D_K \mathbf{u}_L \right)_\Gamma, \\ 2E_v &\geq \frac{h_1}{d} \left(D_I \mathbf{v}_J, \hat{J}^{-1} J^v C_{IJKL}^v D_K \mathbf{v}_L \right)_\Gamma. \end{aligned} \quad (173)$$

We set $\mathbb{Z}_{JK} = \mathbb{Z}_{JK}^u + \mathbb{Z}_{JK}^v$ and obtain

$$2E_I \geq A_u + A_v, \quad (174)$$

where

$$\begin{aligned} A_u &= \frac{h_1}{d} \left(D_I \mathbf{u}_J, \hat{J}^{-1} J^u C_{IJKL}^u D_K \mathbf{u}_L \right)_\Gamma + (\llbracket \mathbf{u} \rrbracket_J, \mathbb{Z}_{JL}^u \llbracket \mathbf{u} \rrbracket_L)_\Gamma \\ &\quad - (\llbracket \mathbf{u} \rrbracket_J, \mathbb{T}_{JL}^u \mathbf{u}_L)_\Gamma, \\ A_v &= \frac{h_1}{d} \left(D_I \mathbf{v}_J, \hat{J}^{-1} J^v C_{IJKL}^v D_K \mathbf{v}_L \right)_\Gamma + (\llbracket \mathbf{u} \rrbracket_J, \mathbb{Z}_{JL}^v \llbracket \mathbf{u} \rrbracket_L)_\Gamma \\ &\quad + (\llbracket \mathbf{u} \rrbracket_J, \mathbb{T}_{JL}^v \mathbf{v}_L)_\Gamma. \end{aligned} \quad (175)$$

We choose \mathbb{Z}_{JK}^u so that A_u is non-negative. Using the definition of \mathbb{T}_{JL} (106) yields

$$(\llbracket \mathbf{u} \rrbracket_J, \mathbb{T}_{JL}^u \mathbf{u}_L)_\Gamma = (\llbracket \mathbf{u} \rrbracket_J, n_I^u C_{IJKL}^u D_K \mathbf{u}_L)_\Gamma = (n_I^u \llbracket \mathbf{u} \rrbracket_J, C_{IJKL}^u D_K \mathbf{u}_L)_\Gamma. \quad (176)$$

Due to the major symmetry of C_{IJKL} (32), we have

$$(n_I^u \llbracket \mathbf{u} \rrbracket_J, C_{IJKL}^u D_K \mathbf{u}_L)_\Gamma = (n_K^u \llbracket \mathbf{u} \rrbracket_L, C_{IJKL}^u D_I \mathbf{u}_J)_\Gamma. \quad (177)$$

Completing the squares in A_u yields

$$\begin{aligned} A_u &= \\ &\frac{h_1}{d} \left(D_I \mathbf{u}_J - \frac{d\hat{J}}{2h_1 J^u} n_I^u \llbracket \mathbf{u} \rrbracket_J, \frac{J^u}{\hat{J}} C_{IJKL}^u \left(D_K \mathbf{u}_L - \frac{d\hat{J}}{2h_1 J^u} n_K^u \llbracket \mathbf{u} \rrbracket_L \right) \right)_\Gamma \\ &\quad - \left(n_I^u \llbracket \mathbf{u} \rrbracket_J, \frac{d\hat{J}}{4h_1 J^u} C_{IJKL}^u n_K^u \llbracket \mathbf{u} \rrbracket_L \right)_\Gamma + (\llbracket \mathbf{u} \rrbracket_J, \mathbb{Z}_{JL}^u \llbracket \mathbf{u} \rrbracket_L)_\Gamma \geq \\ &\quad \left(\llbracket \mathbf{u} \rrbracket_J, \left(\mathbb{Z}_{JL}^u - \frac{d\hat{J}}{4h_1 J^u} n_I^u C_{IJKL}^u n_K^u \right) \llbracket \mathbf{u} \rrbracket_L \right)_\Gamma, \end{aligned} \quad (178)$$

which is non-negative if

$$\mathbb{Z}_{JL}^u = \beta \frac{d\hat{J}}{4h_1 J^u} n_I^u C_{IJKL}^u n_K^u, \quad \beta \geq 1. \quad (179)$$

A similar derivation yields

$$A_v \geq \left(\llbracket \mathbf{u} \rrbracket_J, \left(\mathbb{Z}_{JL}^v - \frac{d\hat{J}}{4h_1 J^v} n_i^v C_{ijkl}^v n_k^v \right) \llbracket \mathbf{u} \rrbracket_L \right)_\Gamma, \quad (180)$$

which is non-negative if

$$\mathbb{Z}_{JL}^v = \beta \frac{d\hat{J}}{4h_1 J^v} n_i^v C_{ijkl}^v n_k^v, \quad \beta \geq 1. \quad (181)$$

We conclude that E_I is non-negative if

$$\mathbb{Z}_{JL} = \mathbb{Z}_{JL}^u + \mathbb{Z}_{JL}^v = \beta \frac{d\hat{J}}{4h_1} \left(\frac{n_i^u C_{ijkl}^u n_k^u}{J^u} + \frac{n_i^v C_{ijkl}^v n_k^v}{J^v} \right), \quad \beta \geq 1. \quad (182)$$

□

In all simulations in this paper, we set $\beta = 1$, i.e., right on the limit of provable stability.

6.1 Self-adjointness

Let $\bar{\Omega} = \Omega_u \cup \Omega_v$ denote the full domain. Introduce the notation

$$w_J = \begin{cases} u_J, & \vec{X} \in \Omega_u \\ v_J, & \vec{X} \in \Omega_v \end{cases} \quad \text{and} \quad \psi_J = \begin{cases} \phi_J, & \vec{X} \in \Omega_u \\ \chi_J, & \vec{X} \in \Omega_v \end{cases}, \quad (183)$$

where we think of w_J as the primal field and ψ_J as the adjoint field. The continuous elastic operator satisfies

$$\mathcal{D}_{JL} w_L = \begin{cases} \partial_i C_{ijkl}^u \partial_k u_L, & \vec{X} \in \Omega_u \\ \partial_i C_{ijkl}^v \partial_k v_L, & \vec{X} \in \Omega_v \end{cases}. \quad (184)$$

Requiring that $\mathcal{D}_{JL} w_L$ be square-integrable over each subdomain leads us to define the space

$$\mathcal{V} = \left\{ w_J \in L^2(\bar{\Omega}) \mid \begin{array}{l} \partial_i C_{ijkl}^u \partial_k u_L \in L^2(\Omega_u) \\ \partial_i C_{ijkl}^v \partial_k v_L \in L^2(\Omega_v) \end{array} \right\}. \quad (185)$$

We further require that w_J satisfies appropriate interface and boundary conditions. We define

$$\mathcal{W} = \left\{ w_J \in \mathcal{V} \mid \begin{array}{l} u_J - v_J = 0 \quad \text{on } \Gamma \\ T_{JL}^u u_L + T_{JL}^v v_L = 0 \quad \text{on } \Gamma \\ L_{JL} w_L = 0 \quad \text{on } \partial \bar{\Omega} \end{array} \right\}, \quad (186)$$

where the boundary operator may be either $L_{JL} = T_{JL} + U_{JL}$, for Robin boundary conditions, or $L_{JL} = \delta_{JL}$, for displacement boundary conditions.

The operator $\mathcal{D}_{JL} : \mathcal{W} \rightarrow L^2(\bar{\Omega})$ is self-adjoint, because integrating by parts twice yields

$$\begin{aligned} (\psi_J, \mathcal{D}_{JL} w_L)_{\bar{\Omega}} &= (\phi_J, T_{JL}^u u_L)_{\Gamma} + (\chi_J, T_{JL}^v v_L)_{\Gamma} \\ &\quad - (T_{JL}^u \phi_L, u_J)_{\Gamma} - (T_{JL}^v \chi_L, v_J)_{\Gamma} \\ &\quad + (\partial_I C_{IJKL}^u \partial_K \phi_L, u_J)_{\Omega_u} + (\partial_I C_{IJKL}^v \partial_K \chi_L, v_J)_{\Omega_v} \\ &= (\mathcal{D}_{JL} \psi_L, w_J)_{\bar{\Omega}} \quad \forall w_J, \psi_J \in \mathcal{W}. \end{aligned} \quad (187)$$

Now consider the discrete elastic operator, including interface SATs. Let

$$\mathbf{w}_J = \begin{bmatrix} \mathbf{u}_J \\ \mathbf{v}_J \end{bmatrix}, \quad \boldsymbol{\psi}_J = \begin{bmatrix} \boldsymbol{\phi}_J \\ \boldsymbol{\chi}_J \end{bmatrix}. \quad (188)$$

Omitting SATs for boundary conditions, the total discrete elastic operator in (159) can be written as

$$\mathbb{D}_{JL}^{tot} = \begin{bmatrix} \mathbb{D}_{IK}^{\Omega_u}(C_{IJKL}^u) + \mathbb{S}_{JL}^{uu} & \mathbb{S}_{JL}^{uv} \\ \mathbb{S}_{JL}^{vu} & \mathbb{D}_{IK}^{\Omega_v}(C_{IJKL}^v) + \mathbb{S}_{JL}^{vv} \end{bmatrix}, \quad (189)$$

where the $\mathbb{S}_{JL}^{..}$ operators correspond to the interface SATs. We define discrete integrals over the full domain as the sum of integrals over the subdomains,

$$(\boldsymbol{\psi}_J, \mathbf{w}_J)_{\bar{\Omega}} = (\boldsymbol{\phi}_J, \mathbf{u}_J)_{\Omega_u} + (\boldsymbol{\chi}_J, \mathbf{v}_J)_{\Omega_v}. \quad (190)$$

Theorem 5. *The total discrete elastic operator \mathbb{D}_{JL}^{tot} , corresponding to the scheme (159), including interface SATs, is self-adjoint, i.e.,*

$$(\boldsymbol{\psi}_J, \mathbb{D}_{JL}^{tot} \mathbf{w}_L)_{\bar{\Omega}} = (\mathbb{D}_{JL}^{tot} \boldsymbol{\psi}_L, \mathbf{w}_J)_{\bar{\Omega}} \quad \forall \boldsymbol{\psi}_J, \mathbf{w}_J. \quad (191)$$

Proof. In deriving the weak form (165), we showed that

$$\begin{aligned} (\boldsymbol{\psi}_J, \mathbb{D}_{JL}^{tot} \mathbf{w}_L)_{\bar{\Omega}} &= (\boldsymbol{\phi}_J, (\mathbb{D}_{IK}^{\Omega_u}(C_{IJKL}^u) + \mathbb{S}_{JL}^{uu}) \mathbf{u}_L + \mathbb{S}_{JL}^{uv} \mathbf{v}_L)_{\Omega_u} \\ &\quad + (\boldsymbol{\chi}_J, (\mathbb{D}_{IK}^{\Omega_v}(C_{IJKL}^v) + \mathbb{S}_{JL}^{vv}) \mathbf{v}_L + \mathbb{S}_{JL}^{vu} \mathbf{u}_L)_{\Omega_v} \\ &= -K_u(\vec{\boldsymbol{\phi}}, \vec{\mathbf{u}}) - K_v(\vec{\boldsymbol{\chi}}, \vec{\mathbf{v}}) + I(\vec{\boldsymbol{\phi}}, \vec{\mathbf{u}}, \vec{\boldsymbol{\chi}}, \vec{\mathbf{v}}), \end{aligned} \quad (192)$$

where we are omitting all terms corresponding to outer boundaries for convenience. Using the symmetries of $K_{u,v}$ and I and the symmetry of $(\cdot, \cdot)_{\bar{\Omega}}$ yields

$$\begin{aligned} (\boldsymbol{\psi}_J, \mathbb{D}_{JL}^{tot} \mathbf{w}_L)_{\bar{\Omega}} &= -K_u(\vec{\boldsymbol{\phi}}, \vec{\mathbf{u}}) - K_v(\vec{\boldsymbol{\chi}}, \vec{\mathbf{v}}) + I(\vec{\boldsymbol{\phi}}, \vec{\mathbf{u}}, \vec{\boldsymbol{\chi}}, \vec{\mathbf{v}}) \\ &= -K_u(\vec{\mathbf{u}}, \vec{\boldsymbol{\phi}}) - K_v(\vec{\mathbf{v}}, \vec{\boldsymbol{\chi}}) + I(\vec{\mathbf{u}}, \vec{\boldsymbol{\phi}}, \vec{\mathbf{v}}, \vec{\boldsymbol{\chi}}) \\ &= (\mathbf{w}_J, \mathbb{D}_{JL}^{tot} \boldsymbol{\psi}_L)_{\bar{\Omega}} = (\mathbb{D}_{JL}^{tot} \boldsymbol{\psi}_L, \mathbf{w}_J)_{\bar{\Omega}}. \end{aligned} \quad (193)$$

□

7 Numerical experiments

This section contains three numerical experiments. First, we use the method of manufactured solutions to assess the global convergence rates of the new SBP-SAT schemes based on the fully compatible operators adapted from Mattsson's operators [27]. Second, we use the new methods to evaluate the performance of an elastodynamic cloak. Third, we solve an application problem inspired by seismic exploration in mountainous regions.

Before presenting the numerical experiments, we briefly discuss how the time step is selected. In anisotropic media the wave speeds are direction-dependent. One may compute the wave speeds in a given direction by finding the roots of a degree d polynomial whose coefficients are functions of density and stiffness [51]. To determine a reasonable time step, we sample the wave speed in five different directions. Let v_{max} denote the largest of those five speeds. This computation is performed with the transformed material parameters, because grid spacing h is well defined in the reference domain. For each grid point, we compute the ratio h/v_{max} . The smallest value of h/v_{max} determines the time-step according to

$$\Delta t = \text{CFL} \times \min_{\text{all gridpoints}} \frac{h}{v_{max}}, \quad (194)$$

where CFL depends on the order of accuracy. Appropriate values of CFL are determined empirically but are generally $\mathcal{O}(1)$.

7.1 Convergence studies

Consider the domain depicted in Figure 2a. We use the method of manufactured solutions and choose the exact solution

$$u_1 = \sin(2X_1 + 3X_2 - t), \quad u_2 = \sin(3X_1 + 2X_2 - 2t), \quad (195)$$

and the material parameters

$$\rho = 2 + \sin\left(\frac{x+y}{2}\right), \quad C_{ijkl} = \begin{cases} \alpha_{ijkl}, & I = K \text{ and } J = L \\ \beta_{ijkl}, & \text{otherwise} \end{cases}, \quad (196)$$

where

$$\alpha_{ijkl} = 8 + \sin(IKX_1 + JX_2) + \frac{1}{2} \sin(KX_1 - LX_2) \quad (197)$$

and

$$\begin{aligned} \beta_{ijkl} = & \frac{1}{8} (\sin(IKX_1 + JX_2) + \sin(KX_1 + LX_2)) \\ & + \frac{1}{16} (\sin(IKX_1 - JX_2) + \sin(KX_1 - LX_2)). \end{aligned} \quad (198)$$

We impose traction conditions on the outer boundaries and displacement conditions on the interior scatterer, and use the exact solution as boundary and initial data. For time-integration we use the classical fourth order

Runge–Kutta method with $\text{CFL} = 0.5$, which proved to be small enough to make the spatial errors dominate. We set $T = 1$ as the final time. Figure 2b and Table 1 show the ℓ^2 errors as functions of h , where h denotes the grid spacing in the reference domain. The convergence rates appear to be 2, 3.5,

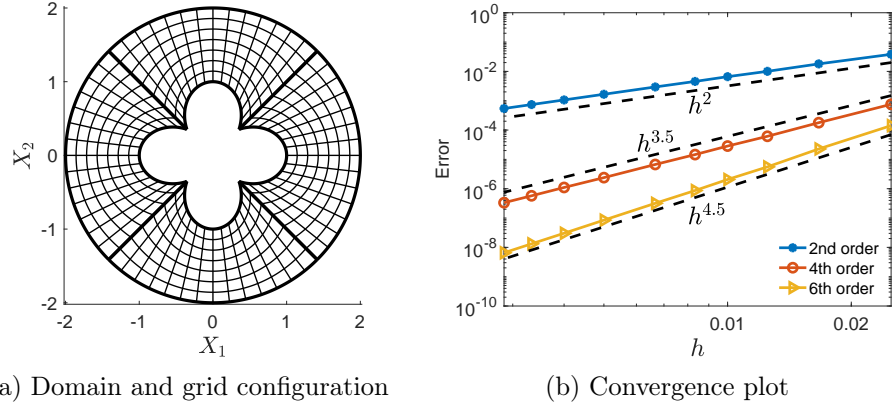


Figure 2: (a) Multiblock grid used in the computations. (b) Convergence plot. h denotes the smallest grid spacing in the reference domain.

and 4.5, for interior orders two, four, and six. Recall that the adapted operators used here have reduced boundary accuracy $q_b = q - 1$. In numerical experiments with second-derivative SBP operators, the convergence rate is often observed to be $\min(q_b + 2, 2q)$. For the adapted operators, this rule of thumb predicts rates 2, 3, and 4, and for operators with full boundary accuracy $q_b = q$, it predicts rates 2, 4, and 5. The second order adapted operator yields rate 2, as predicted by the rule of thumb. For orders four and six, the adapted operators suffer from a reduction by only half an order compared to their $q_b = q$ counterparts. Their rates are half an order higher than predicted by the rule of thumb. Explaining this “super convergence” will have to be the topic of another paper. For now, we conclude that—as fully compatible operators with full boundary accuracy are currently lacking—the adapted operators provide a reasonable compromise that allows for a straightforward stability proof at the cost of no more than half an order reduction of global accuracy.

Although [15] did not observe any accuracy reduction for the adapted operators applied to isotropic materials, we can hereby conclude that schemes based on the adapted operators of orders $2q = 4$ and $2q = 6$ both suffer a reduction by half an order, at least for general anisotropic materials.

7.2 Elastodynamic cloaking

Elastic cloaking is the art of making an object impossible to detect by means of elastic waves by surrounding the object with carefully chosen materials.

| h^{-1} | second order | | fourth order | | sixth order | |
|----------|---------------------------|------|---------------------------|------|---------------------------|------|
| | $\log_{10}(\text{error})$ | r | $\log_{10}(\text{error})$ | r | $\log_{10}(\text{error})$ | r |
| 40 | -1.42 | | -3.12 | | -3.85 | |
| 60 | -1.74 | 1.85 | -3.75 | 3.56 | -4.64 | 4.51 |
| 80 | -2.00 | 2.03 | -4.21 | 3.72 | -5.26 | 4.90 |
| 100 | -2.18 | 1.88 | -4.55 | 3.44 | -5.69 | 4.44 |
| 120 | -2.34 | 2.05 | -4.84 | 3.67 | -6.06 | 4.75 |
| 150 | -2.53 | 1.94 | -5.17 | 3.48 | -6.50 | 4.50 |
| 200 | -2.78 | 1.99 | -5.62 | 3.59 | -7.07 | 4.59 |
| 250 | -2.97 | 2.00 | -5.96 | 3.46 | -7.52 | 4.61 |
| 300 | -3.13 | 2.00 | -6.24 | 3.58 | -7.88 | 4.55 |
| 350 | -3.26 | 2.00 | -6.48 | 3.52 | -8.18 | 4.56 |

Table 1: ℓ^2 errors and convergence rates r .

Perfect cloaking can in theory be achieved by utilizing a coordinate transformation that maps the object to a point, but such transformations are singular and would require singular material properties in the cloak. In practice, one usually settles for *partial* cloaking, where the object is transformed to a much smaller object. Since the equations of Cosserat materials are invariant under coordinate transformation, they allow for cloaking [33, 35], at least at a mathematical level. Not all nonsingular cloaks are realizable in practice, because the material properties prescribed by the coordinate transformation may be infeasible to engineer [18, 19].

As an example, consider a homogeneous isotropic material with material parameters $\rho = 1$ and $\lambda = \mu = 1$, with an embedded scatterer (the scatterer is shown in red in Figure 3b). We model the scatterer as impenetrable by imposing homogeneous displacement conditions on its surface. We let the cloaking region extend from the scatterer to the circle marked by the dashed red line in Figure 3c. Inside the dashed red circle, we apply a coordinate transformation such that the scatterer is mapped to the small disk shown in Figure 3d. To quantify the performance of the cloak, we probe the scatterer by applying a time-harmonic point force outside of the cloak. Similar experiments with circular and spherical cloaks were performed in [8] and [12]. Here, we allow for more complicated objects and cloak shapes. Instead of computing the transformation gradient analytically, we let the grids define the transformation and compute its gradient via numerical differentiation. In the presence of a time-harmonic line force, the 2D equations of motion read

$$\rho \ddot{u}_J = \partial_I C_{IJKL} \partial_K u_L + f_J \delta(\vec{X} - \vec{X}_0) \cos \alpha t, \quad (199)$$

where f_J here is force per unit distance (not force per unit volume as in (11)). We use super-grid absorbing layers [4, 39] to approximate (199) in an

unbounded domain. The semidiscrete system of equations then reads

$$\rho \ddot{\mathbf{u}}_J = (\mathbb{D}_{IK}^\Omega(C_{IJKL}) + \mathbb{S}_{JL}) \mathbf{u}_L + \mathbb{E}_{JL} \dot{\mathbf{u}}_L + f_J \mathbf{d}(\vec{X} - \vec{X}_0) \cos \alpha t, \quad (200)$$

where \mathbb{S}_{JL} denotes the SATs, \mathbf{d} is a discrete approximation of the δ -function [37], and \mathbb{E}_{JL} provides dissipation in the super-grid layers. In the domain of interest, \mathbb{E}_{JL} is zero. Inside the super-grid layers, $H\mathbb{E}_{JL}$ is symmetric negative semidefinite. The time harmonic solution to (200) can be written as

$$\mathbf{u}_J = \mathbf{v}_J \cos \alpha t + \mathbf{w}_J \sin \alpha t. \quad (201)$$

Inserting the ansatz (201) in (200) yields the system of equations

$$\begin{aligned} -\rho \alpha^2 \mathbf{v}_J &= (\mathbb{D}_{IK}^\Omega(C_{IJKL}) + \mathbb{S}_{JL}) \mathbf{v}_L + \alpha \mathbb{E}_{JL} \mathbf{w}_L + f_J \mathbf{d}(\vec{X} - \vec{X}_0), \\ -\rho \alpha^2 \mathbf{w}_J &= (\mathbb{D}_{IK}^\Omega(C_{IJKL}) + \mathbb{S}_{JL}) \mathbf{w}_L - \alpha \mathbb{E}_{JL} \mathbf{v}_L, \end{aligned} \quad (202)$$

which we solve for \mathbf{v}_J and \mathbf{w}_J .

We choose force position $\vec{X}_0 = [1.5, 1.5]$, force vector $\vec{f} = [-\frac{1}{\sqrt{2}}, \frac{1}{\sqrt{2}}]$, angular frequency $\alpha = 2\pi$, and use the sixth order SBP-SAT method to discretize (199). Figure 3a shows the resulting displacement magnitude $\sqrt{\mathbf{v}_1 \circ \mathbf{v}_1 + \mathbf{v}_2 \circ \mathbf{v}_2}$, where \circ denotes the Hadamard product, in free space, with no scatterer present (corresponding plots of $\vec{\mathbf{w}}$ are qualitatively similar and are omitted here). A perfect cloak would yield the same displacement outside of the cloak. Figure 3b shows the displacement field in the presence of the uncloaked scatterer. There are obvious differences compared to the free-space solution—in particular the shadow zone to the southwest of the scatterer. Figure 3c shows the displacement around the cloaked scatterer. Outside the cloak, the displacement is quite similar to the free-space solution, with minor differences—note in particular the faint shadow zone to the southwest of the scatterer. Outside the cloak, the displacement due to the cloaked scatterer is in fact identical (up to numerical errors) to the displacement produced by the small disk-shaped scatterer in Figure 3d, with homogeneous material parameters. In this numerical experiment we could easily improve the performance of the cloak by making the disk in Figure 3d even smaller, but that would make the coordinate transformation near-singular and would likely make the prescribed cloak material more difficult to engineer.

7.3 Seismic imaging in mountainous regions

The topic of the second application problem is seismic imaging on land, in particular in mountainous regions where topographical variations may be large. Other studies that have developed finite difference methods on curvilinear grids for use in seismic imaging in the presence of topography include [45, 46]. As a structural model representative of mountainous regions

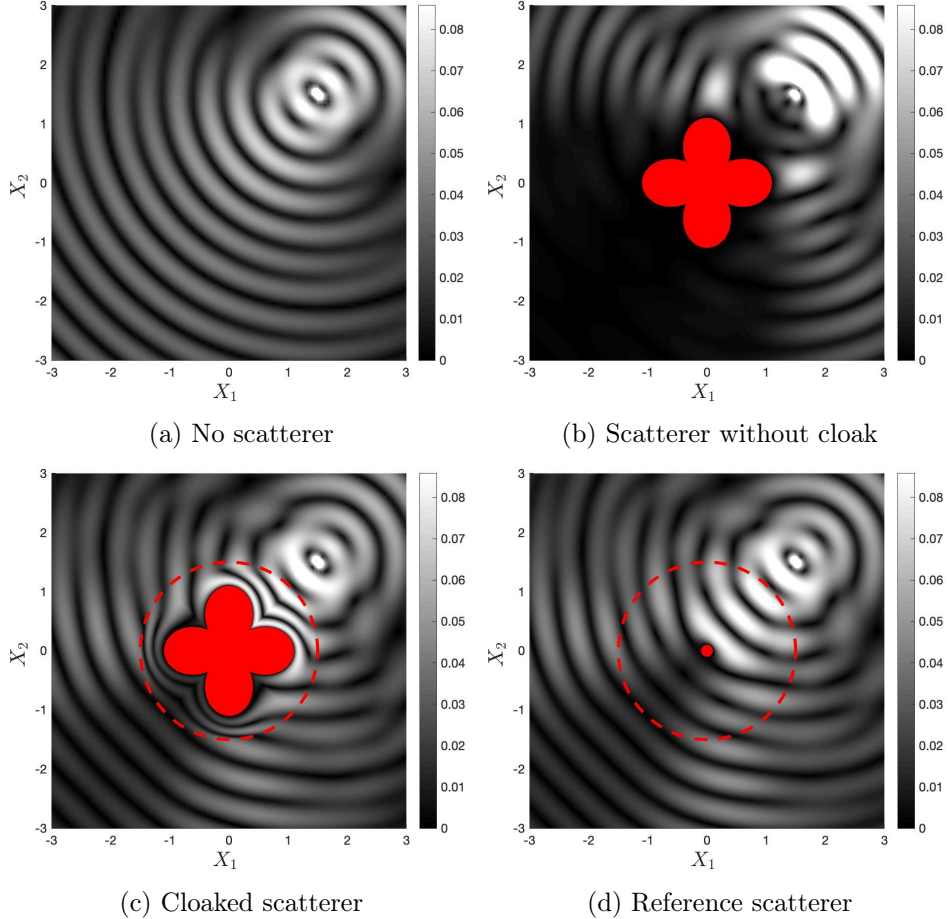
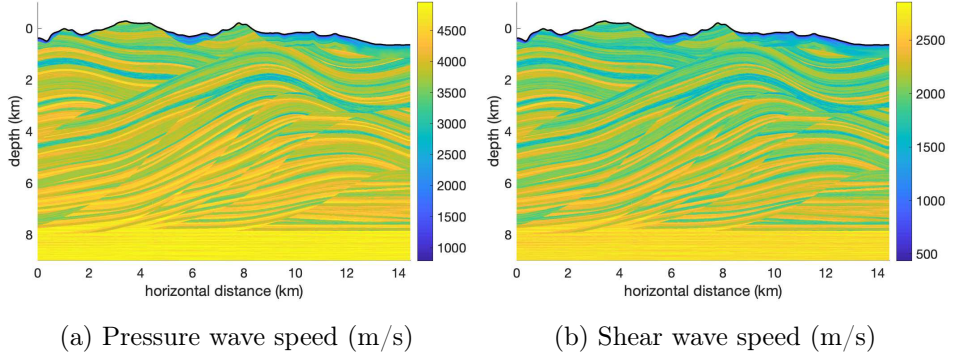


Figure 3: Plots of displacement magnitude $\sqrt{\mathbf{v}_1 \circ \mathbf{v}_1 + \mathbf{v}_2 \circ \mathbf{v}_2}$ caused by a time-harmonic point force applied at $\vec{X} = [1.5, 1.5]$ with (a) no scatterer; (b) an uncloaked scatterer; (c) a cloaked scatterer; and (d) the small reference scatterer that is equivalent to the cloaked scatterer.

we choose the SEG SEAM Foothills model [36], which is an isotropic model with heterogeneous material properties and very pronounced topography. We select a vertical cross section of the original 3D structural model with pressure and shear wave speeds as shown in Figures 4a and 4b. To mimic a vibrator source, we impose homogeneous traction boundary conditions on the free surface and apply a vertical point force at the surface (alternatively, one could impose inhomogeneous traction boundary conditions, which, for a particular choice of the discrete delta function, yields an identical semi-discrete problem). The force vector is (note that we use the symbol δ to denote both the Kronecker delta and the Dirac delta function)

$$f_J = -\delta_{J2} \hat{f} W(t) \delta(\vec{X} - \vec{X}_0), \quad (203)$$



where \hat{f} is a scalar force amplitude and $W(t)$ denotes the Ricker wavelet [41, 42] with peak frequency α centered at time t_0 , i.e.,

$$W(t) = (1 - 2\pi^2\alpha^2(t - t_0)^2)e^{-\pi^2\alpha^2(t - t_0)^2}. \quad (204)$$

We choose $\alpha = 10$ Hz and $t_0 = \alpha^{-1}$ and let the horizontal position of the point force be $X_1 = 6$ km. We select $\hat{\rho} = 1340$ kg/m³ and $\hat{c}_s = 600$ m/s as reference values for density and shear wave speed near the source and define nondimensional particle velocity $\dot{\hat{u}}_1$ as

$$\dot{\hat{u}}_1 = \frac{\hat{\rho}\hat{c}_s^2}{\hat{f}\alpha}\dot{u}_1. \quad (205)$$

Our implementation utilizes the PETSc [7, 5, 6] implementation of the classical fourth order Runge–Kutta method in the TS ODE/DAE solver library [1]. We use the sixth order SBP-SAT method with grid spacing ≈ 7 m (in the physical domain Ω) and set CFL = 0.4. The grid is generated by transfinite interpolation with uniform spacing in the horizontal direction. We again use super-grid absorbing layers at the artificial boundaries. We use only one grid block to discretize the domain shown in Figure 4a and hence differentiate across the discontinuities in material parameters associated with the many media layers. While this constitutes a first order error, we remark that the method remains energy stable.

The top three rows of Figure 5 show snapshots of particle velocity in the vertical direction. The bottom panel shows a space-time plot (shot gather) of vertical particle velocity recorded at the surface. To assess the influence of the structural model, Figure 6 shows similar plots for the case of constant material parameters $\rho = 2300$ kg/m³, pressure wave speed $c_p = 3500$ m/s, and shear wave speed $c_s = 2000$ m/s. Dashed vertical lines in the bottom panel relate scattering of waves to topographical features.

8 Conclusions

We have developed an SBP-SAT method for the anisotropic elastic wave equation on curvilinear multiblock grids in d dimensions. Robin boundary conditions, displacement boundary conditions, and interface conditions are all imposed using SATs, which are designed so that the spatial discretization is energy-stable and self-adjoint. The method assumes fully compatible diagonal-norm SBP operators for variable coefficients. In the numerical experiments, we formed fully compatible operators (here referred to as *adapted* fully compatible operators) by adding a correction to the compatible operators constructed by Mattsson [27]. Although the resulting fully compatible operators are one order less accurate at grid end points, our numerical experiments indicate that the global convergence rate is reduced by only half an order, for orders four and six, and not at all for order two. The convergence rates are 2, 3.5, and 4.5, for interior orders two, four and six.

We have applied the new method to problems inspired by elastodynamic cloaking and seismic imaging. In elastodynamic cloaking, anisotropic materials are essential. Hence methods such as ours, which can handle general anisotropy, are the key to evaluating the performance of proposed cloaks via numerical simulation. In the seismic imaging experiment we considered the SEAM Foothills velocity model [36], which features large variations in elevation. Our method offers accurate approximation of the topography and the free surface boundary condition, both of which are necessary to model the highly complex surface waves accurately.

MATLAB code that reproduces figures 1, 2, and 3 is available at
<https://sourceforge.net/projects/elastic-curvilinear/>

Acknowledgments

We thank Joe Stefani for useful discussions of seismic imaging and help with the Foothills model. M. Almquist gratefully acknowledges support from the Knut and Alice Wallenberg Foundation (Dnr. KAW 2016.0498).

References

- [1] S. Abhyankar, J. Brown, E. M. Constantinescu, D. Ghosh, B. F. Smith, and H. Zhang. PETSc/TS: A modern scalable ODE/DAE solver library. *arXiv:1806.01437 [math.NA]*, 2018. URL <https://arxiv.org/abs/1806.01437>.
- [2] M. Almquist and E. M. Dunham. Non-stiff boundary and interface penalties for narrow-stencil finite difference approximations of the Laplacian on curvilinear multiblock grids. *J. Comput. Phys.*, 408, 2020. doi:10.1016/j.jcp.2020.109294.

- [3] M. Almquist, S. Wang, and J. Werpers. Order-preserving interpolation for summation-by-parts operators at non-conforming grid interfaces. *SIAM J. Sci. Comput.*, 41(2):A1201–A1227, 2019. URL <https://doi.org/10.1137/18M1191609>.
- [4] D. Appelö and T. Colonius. A high-order super-grid-scale absorbing layer and its application to linear hyperbolic systems. *J. Comput. Phys.*, 228:4200–4217, 2009. doi:10.1016/j.jcp.2009.02.030.
- [5] S. Balay, S. Abhyankar, M. F. Adams, J. Brown, P. Brune, K. Buschelman, L. Dalcin, A. Dener, V. Eijkhout, W. D. Gropp, D. Karpeyev, D. Kaushik, M. G. Knepley, D. A. May, L. C. McInnes, R. T. Mills, T. Munson, K. Rupp, P. Sanan, B. F. Smith, S. Zampini, H. Zhang, and H. Zhang. PETSc users manual. Technical Report ANL-95/11 - Revision 3.12, Argonne National Laboratory, 2019. URL <https://www.mcs.anl.gov/petsc>.
- [6] S. Balay, S. Abhyankar, M. F. Adams, J. Brown, P. Brune, K. Buschelman, L. Dalcin, A. Dener, V. Eijkhout, W. D. Gropp, D. Karpeyev, D. Kaushik, M. G. Knepley, D. A. May, L. C. McInnes, R. T. Mills, T. Munson, K. Rupp, P. Sanan, B. F. Smith, S. Zampini, H. Zhang, and H. Zhang. PETSc Web page, 2019. URL <https://www.mcs.anl.gov/petsc>.
- [7] S. Balay, W. D. Gropp, L. C. McInnes, and B. F. Smith. Efficient management of parallelism in object oriented numerical software libraries. In E. Arge, A. M. Bruaset, and H. P. Langtangen, editors, *Modern Software Tools in Scientific Computing*, pages 163–202. Birkhäuser Press, 1997.
- [8] M. Brun, S. Guenneau, and A. B. Movchan. Achieving control of in-plane elastic waves. *Appl. Phys. Lett.*, 94(6):10–13, 2009. doi:10.1063/1.3068491.
- [9] M. H. Carpenter, D. Gottlieb, and S. Abarbanel. Time-stable boundary conditions for finite-difference schemes solving hyperbolic systems: Methodology and application to high-order compact schemes. *J. Comput. Phys.*, 111(2):220–236, 1994. URL <https://doi.org/10.1006/jcph.1994.1057>.
- [10] E. Cosserat and F. Cosserat. *Théorie des corps déformables (English version: Theory of deformable bodies, NASA TT F-11 561 (1968))*. A. Hermann et fils, Paris, 1909.
- [11] D. C. Del Rey Fernández, J. E. Hicken, and D. W. Zingg. Review of summation-by-parts operators with simultaneous approximation terms

for the numerical solution of partial differential equations. *Comput. Fluids*, 95:171–196, 2014. doi:10.1016/j.compfluid.2014.02.016.

- [12] A. Diatta and S. Guenneau. Controlling solid elastic waves with spherical cloaks. *Appl. Phys. Lett.*, 105(2), 2014. doi:10.1063/1.4887454.
- [13] L. Dovgilovich and I. Sofronov. High-accuracy finite-difference schemes for solving elastodynamic problems in curvilinear coordinates within multiblock approach. *Appl. Numer. Math.*, 93:176–194, 2015. doi:10.1016/j.apnum.2014.06.005.
- [14] K. Duru, G. Kreiss, and K. Mattsson. Stable and high-order accurate boundary treatments for the elastic wave equation on second-order form. *SIAM J. Sci. Comput.*, 36(6):A2787–A2818, 2014. doi:10.1137/130947210.
- [15] K. Duru and K. Virta. Stable and high order accurate difference methods for the elastic wave equation in discontinuous media. *J. Comput. Phys.*, 279:37–62, 2014. doi:10.1016/j.jcp.2014.08.046.
- [16] T. H. Fisher and M. H. Carpenter. High-order entropy stable finite difference schemes for nonlinear conservation laws: Finite domains. *J. Comput. Phys.*, 252:518–557, 2013. doi:10.1016/j.jcp.2013.06.014.
- [17] L. Gao and D. Keyes. Combining finite element and finite difference methods for isotropic elastic wave simulations in an energy-conserving manner. *J. Comput. Phys.*, 378:665–685, 2019. doi:10.1016/j.jcp.2018.11.031.
- [18] M. Kadic, T. Bückmann, R. Schittny, and M. Wegener. On anisotropic versions of three-dimensional pentamode metamaterials. *New J. Phys.*, 15, 2013. doi:10.1088/1367-2630/15/2/023029.
- [19] M. Kadic, T. Bückmann, N. Stenger, M. Thiel, and M. Wegener. On the practicability of pentamode mechanical metamaterials. *Appl. Phys. Lett.*, 100, 2012. doi:10.1063/1.4709436.
- [20] J. E. Kozdon, E. M. Dunham, and J. Nordström. Interaction of Waves with Frictional Interfaces Using Summation-by-Parts Difference Operators: Weak Enforcement of Nonlinear Boundary Conditions. *J. Sci. Comput.*, 50(2):341–367, 2011. doi:10.1007/s10915-011-9485-3.
- [21] J. E. Kozdon, E. M. Dunham, and J. Nordström. Simulation of dynamic earthquake ruptures in complex geometries using high-order finite difference methods. *J. Sci. Comput.*, 55(1):92–124, 2013. doi:10.1007/s10915-012-9624-5.

- [22] H.-O. Kreiss and J. Oliger. Comparison of accurate methods for the integration of hyperbolic equations. *Tellus*, XXIV:199–215, 1972. URL <https://doi.org/10.3402/tellusa.v24i3.10634>.
- [23] H.-O. Kreiss, N. A. Petersson, and J. Yström. Difference approximations for the second order wave equation. *SIAM J. Num. Anal.*, 40:1940–1967, 2002. URL <https://doi.org/10.1137/S0036142901397435>.
- [24] H.-O. Kreiss and G. Scherer. Finite element and finite difference methods for hyperbolic partial differential equations. *Mathematical Aspects of Finite Elements in Partial Differential Equations.*, Academic Press, Inc., pages 195–212, 1974. URL <https://doi.org/10.1016/B978-0-12-208350-1.50012-1>.
- [25] T. Lundquist, A. Malan, and J. Nordström. A hybrid framework for coupling arbitrary summation-by-parts schemes on general meshes. *J. Comput. Phys.*, 362:49–68, 2018. doi:10.1016/j.jcp.2018.02.018.
- [26] L. E. Malvern. *Introduction to the Mechanics of a Continuous Medium*. Prentice-Hall, Inc., 1969.
- [27] K. Mattsson. Summation by parts operators for finite difference approximations of second-derivatives with variable coefficients. *J. Sci. Comput.*, 51:650–682, 2012. doi:10.1007/s10915-011-9525-z.
- [28] K. Mattsson and M. H. Carpenter. Stable and accurate interpolation operators for high-order multi-block finite-difference methods. *SIAM J. Sci Comput.*, 32(4):2298–2320, 2010. doi:10.1137/090750068.
- [29] K. Mattsson and J. Nordström. Summation by parts operators for finite difference approximations of second derivatives. *J. Comput. Phys.*, 199(2):503–540, 2004. URL <https://doi.org/10.1016/j.jcp.2004.03.001>.
- [30] K. Mattsson and F. Parisi. Stable and accurate second-order formulation of the shifted wave equation. *Commun. Comput. Phys.*, 7:103–137, 2010. doi:10.4208/cicp.2009.08.135.
- [31] G. W. Milton, M. Briane, and J. R. Willis. On cloaking for elasticity and physical equations with a transformation invariant form. *New J. Phys.*, 8, 2006. doi:10.1088/1367-2630/8/10/248.
- [32] G. W. Milton and J. R. Willis. On modifications of Newton’s second law and linear continuum elastodynamics. *Proceedings of the Royal Society A: Mathematical, Physical and Engineering Sciences*, 463(2079):855–880, 2007. doi:10.1098/rspa.2006.1795.

- [33] A. N. Norris and A. L. Shuvalov. Elastic cloaking theory. *Wave Motion*, 48(6):525–538, 2011. doi:10.1016/j.wavemoti.2011.03.002.
- [34] P. Olsson. *High-order difference methods and dataparallel implementation*. Ph.D. thesis, Dept. of Scientific Computing, Uppsala University, 1992.
- [35] P. Olsson and D. J. N. Wall. Partial elastodynamic cloaking by means of fiber-reinforced composites. *Inverse Probl.*, 27(4), 2011. doi:10.1088/0266-5611/27/4/045010.
- [36] M. Oristaglio. SEAM phase II: the Foothills model—seismic exploration in mountainous regions. *The Leading Edge*, 35(10):1020–1024, 2016. doi:10.1190/tle35100912.1.
- [37] N. A. Petersson, O. O'Reilly, B. Sjögreen, and S. Bydlon. Discretizing singular point sources in hyperbolic wave propagation problems. *J. Comput. Phys.*, 321:532–555, 2016. doi:10.1016/j.jcp.2016.05.060.
- [38] N. A. Petersson and B. Sjögreen. Wave propagation in anisotropic elastic materials and curvilinear coordinates using a summation-by-parts finite difference method. *J. Comput. Phys.*, 299:820–841, 2015. doi:10.1016/j.jcp.2015.07.023.
- [39] N. A. Petersson and B. Sjögreen. Super-grid modeling of the elastic wave equation in semi-bounded domains. *Commun. Comput. Phys.*, 16(4):913–955, 2014. doi:10.4208/cicp.290113.220514a.
- [40] Y. Rao and Y. Wang. Seismic waveform simulation for models with fluctuating interfaces. *Sci. Rep.*, 8, 2018. doi:10.1038/s41598-018-20992-z.
- [41] N. Ricker. Further developments in the wavelet theory of seismogram structure. *B. Seismol. Soc. Am.*, 33(3):197–228, 1943, <https://pubs.geoscienceworld.org/bssa/article-pdf/33/3/197/2690607/BSSA0330030197.pdf>.
- [42] N. Ricker. Wavelet Functions and Their Polynomials. *Geophysics*, 9(3):314–323, 1944. doi:10.1190/1.1445082.
- [43] W. Rudin. *Functional Analysis*. McGraw-Hill Book Company, 1973.
- [44] G. Scherer. *On the existence of energy estimates for difference approximations for hyperbolic systems*. Ph.D. thesis, Dept. of Scientific Computing, Uppsala University, 1977.
- [45] J. Shragge. Acoustic wave propagation in tilted transversely isotropic media: Incorporating topography. *Geophysics*, 81(5), 2016. doi:10.1190/geo2015-0311.1.

- [46] J. Shragge and B. Tapley. Solving the tensorial 3D acoustic wave equation: A mimetic finite-difference time-domain approach. *Geophysics*, 82(4), 2017. doi:10.1190/geo2016-0691.1.
- [47] B. Strand. Summation by parts for finite difference approximations for d/dx . *J. Comput. Phys.*, 110:47–67, 1994. doi:10.1006/jcph.1994.1005.
- [48] C. Sun, Z.-L. Yang, G.-X.-X. Jiang, and Y. Yang. Multiblock SBP-SAT Methodology of Symmetric Matrix Form of Elastic Wave Equations on Curvilinear Grids. *Shock Vib.*, 2020. doi:10.1155/2020/8401537.
- [49] M. Svärd and J. Nordström. On the order of accuracy for difference approximations of initial-boundary value problems. *J. Comput. Phys.*, 218:333–352, 2006. URL <https://doi.org/10.1016/j.jcp.2006.02.014>.
- [50] M. Svärd and J. Nordström. Review of summation-by-parts schemes for initial-boundary-value problems. *J. Comput. Phys.*, 268:17–38, 2014. doi:<http://dx.doi.org/10.1016/j.jcp.2014.02.031>.
- [51] J. L. Synge. Elastic Waves in Anisotropic Media. *J. Math. Phys.*, 35(1-4):323–334, 1956. doi:10.1002/sapm1956351323.
- [52] J. F. Thompson, Z. U. Warsi, and C. W. Mastin. *Numerical grid generation: foundations and applications*, volume 45. North-holland Amsterdam, 1985. URL <http://www.hpc.msstate.edu/publications/gridbook/cover.php>.

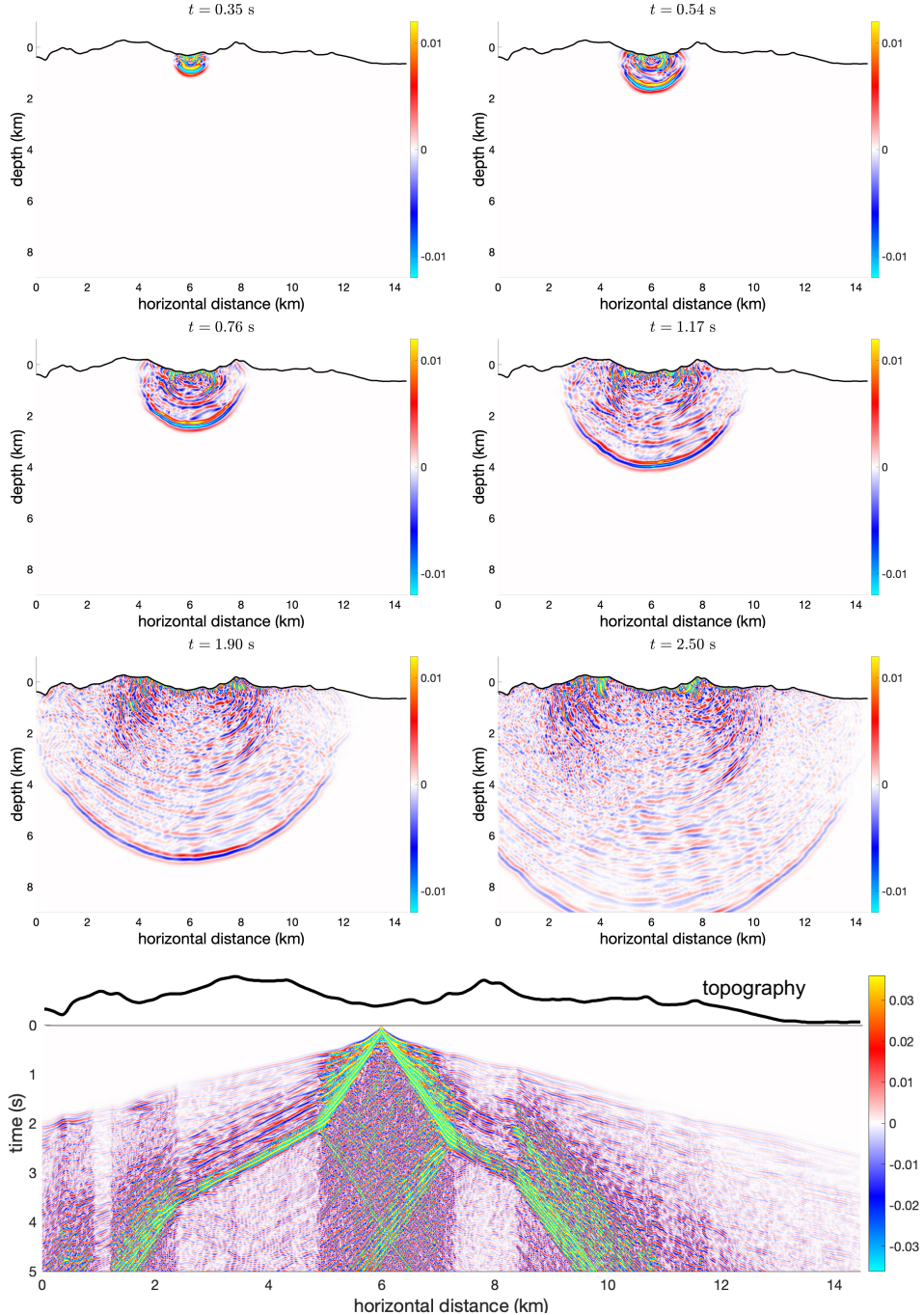


Figure 5: Plots of \dot{u}_2 , the vertical component of particle velocity with the Foothills structural model. The top three rows show snapshots of \dot{u}_2 at different times. The bottom panel shows a space-time plot (shot gather) of \dot{u}_2 , recorded at the surface.

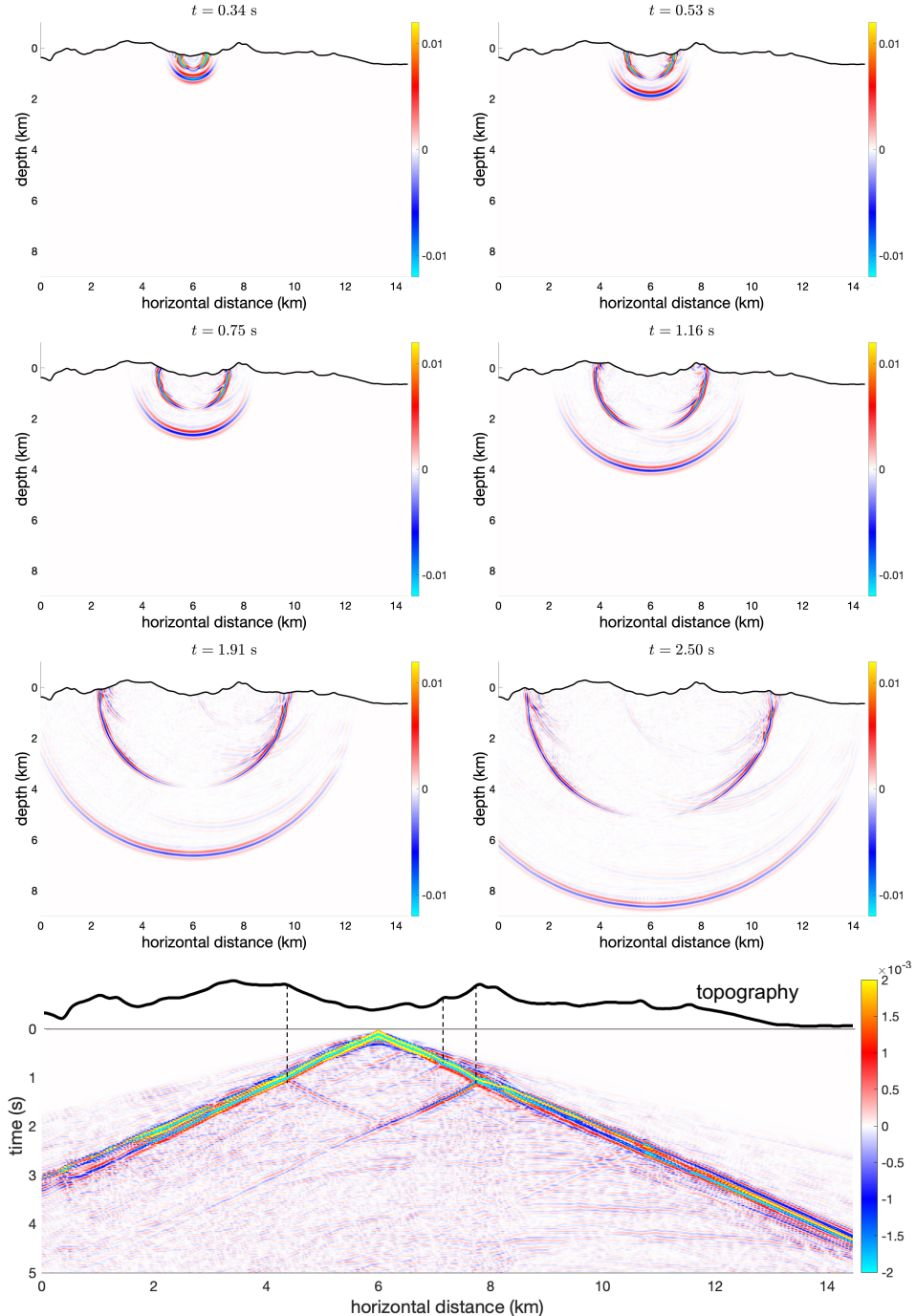


Figure 6: Plots of \dot{u}_2 , the vertical component of particle velocity, with constant material parameters. The top three rows show snapshots of \dot{u}_2 at different times. The bottom panel shows a space-time plot (shot gather) of \dot{u}_2 , recorded at the surface. Dashed vertical lines in the space-time plot relate wave scattering to topographical features.